https://doi.org/10.5194/egusphere-2026-3344
Preprint. Discussion started: 14 July 2026

ENSO Teleconnection Patterns Modulate Australian Extratropical Cyclones

Linyuan Sun[1,2], Andréa S. Taschetto[1,2], Shayne McGregor[3,4], Lisa V. Alexander[1,2], and Chenhui Jin[3,4]

[1]Climate Change Research Centre, University of New South Wales, Sydney, Australia
[2]ARC Centre of Excellence for the Weather of the 21st Century, University of New South Wales, Sydney, Australia
[3]School of Earth, Atmosphere and Environment, Monash University, Clayton, Australia
[4]ARC Centre of Excellence for the Weather of the 21st Century, Monash University, Clayton, Australia

Correspondence to: Linyuan Sun (linyuan.sun@unsw.edu.au)

Abstract. While the effects of the El Niño-Southern Oscillation (ENSO) on Australian rainfall are well known, its modulation of the main rain-producing weather system—extratropical cyclones—is still not well understood. In particular, there is a lack of direct evidence for ENSO-related changes in cyclone day frequency around Australia because high internal variability makes it hard to detect the signal when calculating cyclone frequency under conventional seasonal windows. Given that ENSO influences the extratropics primarily through atmospheric teleconnections, its impact on extratropical cyclones should be detectable on days when teleconnections are well established. Focusing on the austral spring, when the strongest response to ENSO in the southern extratropics is exhibited, we identify persistent teleconnection pattern periods by projecting daily low-frequency circulation fields onto ENSO-composited teleconnection patterns. We then use these days as a sample space to calculate cyclone day frequency. Under this conditioning, we reveal that ENSO teleconnection patterns modulate Southern Hemisphere cyclone activity, with particular signals emerging over the Tasman Sea, where cyclone frequency increases (decreases) up to about 10% during La Niña (El Niño). Tracking statistics further indicate enhanced cyclogenesis over the Tasman Sea during La Niña, and reduced genesis during El Niño, especially for the Central Pacific type. Cyclone residence time over this region also tends to increase during La Niña, consistent with the associated favourable dynamical and moisture environment. Decomposing rainfall anomalies into Tasman Sea cyclone and non-cyclone components further highlights the role of cyclone activity changes in eastern Australian rainfall anomalies during ENSO events. These results suggest the importance of low-frequency circulation regimes in mediating tropical forcing on extratropical weather and provide new insights into the ENSO-weather systems linkage study.

https://doi.org/10.5194/egusphere-2026-3344
Preprint. Discussion started: 14 July 2026

1 Introduction

The El Niño-Southern Oscillation (ENSO) is one of the major remote drivers of Australian climate variability (Risbey et al., 2009; Santoso et al., 2019; Taschetto et al., 2025). Over the last century, numerous studies have examined ENSO's influences on Australia, particularly on rainfall (McBride and Nicholls, 1983; Murphy and Timbal, 2008; Walker, 1925). ENSO variability is closely associated with extreme events such as droughts (Grant et al., 2025; Holgate et al., 2025), floods (Verdon et al., 2004; Wu and Leonard, 2019), and wildfires (Mariani et al., 2016; Williams and Karoly, 1999), with substantial socio-economic impacts in this country. It is widely known that the ENSO-related Australian seasonal rainfall anomalies are typically characterized by the "El Niño-dry and La Niña-wet" relationship (McGregor et al., 2024; van Rensch et al., 2026). In terms of influencing mechanisms, ENSO modulates the tropical Walker circulation and convective heating anomalies (Bjerknes, 1969; Taschetto et al., 2020; Trenberth et al., 1998), which excite Rossby waves that propagate into the extratropics (Hoskins and Karoly, 1981), causing large-scale circulation anomalies projected onto the Pacific-South American (PSA)-like pattern (Karoly, 1989; Mo, 2000; Mo and Higgins, 1998). These atmospheric teleconnections provide the fundamental pathway through which ENSO influences Australian climate. In recent decades, substantial progress has also been made in understanding the complexity of ENSO's seasonal impacts on Australia, including the diversity and asymmetry of ENSO influences (Ma et al., 2023; Sun et al., 2026; Wang et al., 2022), interactions with other climate modes (Cai et al., 2011; Cowan et al., 2023; Ummenhofer et al., 2011), and modulation by multidecadal variability (Power et al., 1999; Trascasa-Castro et al., 2023).

Beyond seasonal-mean climate, an increasing number of studies have investigated how ENSO modulates the statistics of synoptic-scale weather systems, reflecting a growing interest in linking weather and climate (Dole, 2008; Randall and Emanuel, 2024). In Australia, the main rain-producing weather systems are cyclonic low-pressure systems (Dowdy et al., 2013; Pepler and Dowdy, 2021; Pook et al., 2006), with extratropical cyclones and their associated warm conveyor belts (WCBs) acting as major contributors to seasonal rainfall, and their occurrence changes have been shown to explain a substantial fraction of rainfall anomalies in southeastern Australia (Jin et al., 2024, 2025). Despite the well-known influence of ENSO on Australian rainfall and the importance of synoptic-scale cyclonic systems in producing rain, direct evidence supporting the linkage between ENSO and Australian extratropical cyclones is absent. In contrast to tropical cyclones, which are more directly affected by ENSO (Chand et al., 2019; Nicholls, 1979; Ramsay et al., 2014), it is less clear how Australian extratropical cyclones are modulated by ENSO. For example, Australian east coast lows, typical extratropical cyclonic systems that are occasionally associated with upper-level cutoff lows, play a key role in cool-season rainfall variability (Pepler et al., 2014b), yet their relationship with ENSO is generally found to be weak on monthly to seasonal timescales in terms of their frequency, duration, and location (Grosfeld et al., 2021; Pepler et al., 2014b; Pepler and Dowdy, 2021).

Given the chaotic nature of synoptic weather systems on long timescales and the strong internal variability of extratropical atmosphere (Deser et al., 2017; Lorenz, 1963), the absence of a clear ENSO-cyclone relationship reflects a low signal-to-noise ratio in this cross-scale problem and is perhaps unsurprising. Nonetheless, some recent studies provide insightful clues for

https://doi.org/10.5194/egusphere-2026-3344
Preprint. Discussion started: 14 July 2026

further exploring this issue. For example, Hauser et al., (2020) clustered monthly rainfall anomalies in southeastern Australia during El Niño years, identifying a dominant “Dry Cluster 2” that exhibits the typical El Niño-related rainfall decrease pattern. Crucially, this cluster was associated with fewer cyclones and WCBs over the eastern Australian and the Tasman Sea. Another relevant study by Gillett et al., (2023) compared cyclone-day composites with seasonal-mean circulation anomalies during ENSO years and found strong similarities between the two, suggesting that ENSO modulates cyclone statistics through large-scale circulation patterns. Thus, these results motivate us to rethink the possible connection between ENSO and extratropical cyclones over the Australian region. A key question is whether ENSO truly has no significant influence on Australian extratropical cyclones, or whether its impact is obscured by noise and therefore difficult to detect under conventional seasonal analysis.

Answering this question requires a deep understanding of ENSO atmospheric teleconnections (Taschetto et al., 2020), which play a central role in linking tropical forcing and extratropical weather. These teleconnections are essentially low-frequency circulation variability modulated by ENSO-induced tropical heating anomalies (Hannachi et al., 2017; Mo, 2000), also manifested as forced, quasi-stationary planetary waves (Held et al., 2002; Hoerling and Kumar, 2002; Hoskins and Karoly, 1981). Although they exhibit well-organized spatial patterns on seasonal-mean fields, it does not mean that they persist steadily throughout a season. Instead, evidence suggests that they occur episodically on daily scales—the exact timescale on which synoptic weather systems work (Feldstein, 2000; Jaffe et al., 2011). This intraseasonal intermittency of extratropical teleconnections is partly related to the transient nature of tropical convective heating (Matthews and Kiladis, 1999; Stan et al., 2017). While the change in seasonal-mean tropical heating is caused by ENSO-related sea surface temperature (SST) anomalies on seasonal-to-interannual timescales, Branstator (2014) uses atmospheric general circulation model experiments with short-lived tropical heating to demonstrate that the response to steady forcing is essentially the sum of responses to a sequence of heat pulses, and importantly, that short-lived tropical heating can also produce persistent responses in midlatitude circulation and in the statistics of synoptic eddies. These results provide an advanced understanding on the linkage between weather and climate under ENSO conditions.

It is important to note that low-frequency circulation variability in the extratropical atmosphere is strongly coupled with high-frequency variability, or synoptic-scale eddies which are often manifested as propagating weather systems (Tamarin-Brodsky et al., 2026). As a result, extratropical low-frequency variability is not only influenced by tropical forcing associated with SST anomalies such as ENSO, but is also significantly affected by the feedback from synoptic eddies (Karoly, 1990; Lau and Holopainen, 1984), thus forming a two-way dynamical interaction (Jin et al., 2006). Nevertheless, this does not preclude the feasibility of examining the ENSO modulation on high-frequency synoptic systems through teleconnection patterns. Many studies researching low-frequency variability have conducted synoptic analysis on the identification, evolution, and dynamics of low-frequency teleconnection patterns mostly in the Northern Hemisphere, such as the Pacific-North America (PNA) and the North Atlantic Oscillation (NAO) (Benedict et al., 2004; Franzke et al., 2011; Song, 2018). However, the identification of ENSO-related teleconnection patterns on synoptic timescales in the Southern Hemisphere, particularly for distinct Eastern

https://doi.org/10.5194/egusphere-2026-3344
Preprint. Discussion started: 14 July 2026

Pacific (EP) and Central Pacific (CP) El Niño events, as well as La Niña, has received less attention. Consequently, how these teleconnection patterns modulate extratropical cyclones also remains poorly understood.

The teleconnection patterns seen in seasonal-mean fields can be interpreted as the aggregate of episodic events associated with dominant low-frequency variability on synoptic timescales, which implies that ENSO-related changes in synoptic-scale extratropical cyclones, particularly regional signals over Australia, may also occur episodically while are not easily detected in seasonal-mean analysis. Motivated by this, we aim to extract teleconnection pattern periods to examine ENSO modulation of Australian extratropical cyclones. Here we focus on the austral spring (Sep-Oct-Nov, SON) because this season is known to exhibit the strongest seasonal response of Southern Hemisphere extratropical circulation to ENSO. Specifically, teleconnection pattern days are identified by projecting daily low-frequency circulation fields onto ENSO-composited springtime teleconnection patterns, thereby constructing a refined sample space representing periods when ENSO-related teleconnections are well established on daily timescales. Cyclone statistics are then evaluated within these days to possibly enhance the detectability of ENSO-related signals. Among various metrics, cyclone day frequency (CDF) is investigated as a priority, as it provides a clear spatial measure that facilitates the identification of cyclone activity changes hotspots.

Based on the above introduction, the three central questions of this study are therefore as follows:

(1) How are ENSO-related teleconnection patterns in the Southern Hemisphere manifested on daily timescales?

(2) Do Australian extratropical cyclone statistics exhibit a clearer ENSO response when conditioned on these pattern days?

(3) What is the role of cyclone changes in ENSO-related rainfall anomalies over Australia?

The remainder of this paper is organized as follows. Section 2 describes the data and methodology, Section 3 presents the main results addressing the above questions, and Section 4 summarizes and discusses the main findings.

https://doi.org/10.5194/egusphere-2026-3344
Preprint. Discussion started: 14 July 2026

2 Data and methods

2.1 Observations and ERA5 reanalysis

Meteorological fields are derived from the ECMWF Reanalysis v5 (ERA5) (Hersbach et al., 2020), including geopotential height, horizontal wind, vertical velocity, relative vorticity, and vertically integrated moisture flux, all re-gridded to 1° resolution. Sea surface temperature (SST) data are taken from the Hadley Centre Sea Ice and Sea Surface Temperature (HadISST) dataset (Rayner et al., 2003). Tropical convection is represented by interpolated outgoing longwave radiation (OLR) from the National Oceanic and Atmospheric Administration (NOAA) (Liebmann and Smith, 1996). Daily rainfall over Australia is obtained from the Australian Gridded Climate Data (AGCD) at a 0.05° horizontal resolution (Evans et al., 2020). AGCD is constructed from station observations across Australia and is a widely used dataset for weather and climate studies in this country. The analysis timespan in this study is post-satellite era 1979-2022. To reduce the possible influence of decadal variability, daily (monthly) anomalies are derived by subtracting a centered 31-yr sliding climatology for the corresponding calendar day (month), with the anomalies for the first and last 16 years based on a fixed 31-yr window due to data limitation on boundaries. All anomalies are then detrended to remove the long-term linear trend.

2.2 Objectively identified cyclone dataset

Surface cyclones are objectively defined from ERA5 based on the identification and tracking algorithm by Sprenger et al. (2017), which is a modified version of the method proposed by Wernli and Schwierz (2006). A cyclone is identified as an area comprising a local sea level pressure (SLP) minimum, enclosed by the outermost closed SLP contour. Cyclone tracks are constructed by linking SLP minima positions (latitude/longitude) at consecutive hourly time steps. It should be noted that this SLP-based algorithm does not distinguish between different cyclone types. A detailed description of this algorithm is provided in Sprenger et al. (2017). A comprehensive comparison of different extratropical cyclone tracking algorithms, including this SLP-based scheme, can be found in Neu et al. (2013).

The identified cyclone objects are available as hourly two-dimensional binary fields, in which a flag of 1 denotes a grid point covered by a cyclone and 0 otherwise. Further, the hourly binary flag is aggregated to the daily for facilitating the CDF calculation at daily timescale: a grid point is defined as a “cyclone day” if it is flagged for more than 6 hours within a given calendar day (24 hours). We’ve tested 10- and 12-hour thresholds to confirm that the results are robust to this choice. Due to the data availability, this cyclone dataset currently spans 1979-2022 and does not include the recent strong El Niño event of 2023-2024. But the exclusion of this recent year is not expected to substantially affect the overall results.

https://doi.org/10.5194/egusphere-2026-3344
Preprint. Discussion started: 14 July 2026

2.3 EP/CP ENSO events

Since we aim to examine the austral springtime response to ENSO, we consider the SST anomalies in the SON season when identifying ENSO events. Based on the Oceanic Niño Index (ONI) provided by the NOAA Climate Prediction Center, an El Niño (La Niña) event is identified when ONI values from SON of a given year through the following DJF remain above 0.5 (below -0.5), and the value in SON exceed 0.7 (below -0.7). This can effectively identify typical ENSO events while excluding weak cases. On this basis, El Niño events are further classified into EP and CP types following Kug et al. (2009). The EP (CP) El Niño is defined when the SON Niño-3 index is greater (less) than the Niño-4 index. The Niño-3 and Niño-4 indices are calculated as SST anomalies averaged over the Niño-3 (150°W-90°W, 5°N-5°S) and Niño-4 (160°E-150°W, 5°N-5°S) regions, respectively. The resulting classification of events is summarized in Table 1. It should be noted that while the Relative ONI (RONI) has been introduced recently (L'Heureux et al., 2024), the conventional ONI is retained here for identifying typical ENSO events, which are not expected to be sensitive to the index used.

Table 1. Typical ENSO events from the 1980s onwards are classified by the SON-based Niño-3–4 index method. Event years are defined by the corresponding SON season.

ENSO type	Event years
EP El Niño (5)	1982, 1987, 1997, 2006, 2015
CP El Niño (6)	1986, 1991, 1994, 2002, 2009, 2018
La Niña (11)	1983, 1988, 1995, 1998, 1999, 2007, 2010, 2011, 2020, 2021, 2022

2.4 Identification of ENSO teleconnection pattern periods

Because ENSO-related teleconnection patterns are not necessarily maintained throughout the season but instead occur episodically on the daily timescale, the spatial projection-based method (Franzke et al., 2011; Li and Lau, 2012; Song, 2018) is applied to identify the persistent periods exhibiting teleconnection patterns associated with EP El Niño, CP El Niño, and La Niña events.

Specifically, first, the ENSO-composited 500-hPa geopotential height (Z500) anomaly patterns in the SON season over the domain spanning extratropical Australia to the South Pacific (20°S-80°S, 80°E-80°W) are used as the reference patterns. The same domain is adopted for all three ENSO types to ensure comparability (red boxes in Fig. 1g-i). Daily low-frequency Z500 anomaly fields, obtained using a 10-day Lanczos low-pass filter (Duchon, 1979), are then projected onto the reference patterns for each year, yielding the daily timeseries of projection coefficients. The resulting projection coefficients are further normalized by the standard deviation of the entire timeseries over the 1979-2022 to obtain the *daily pattern index* (Fig. S1), which represents the day-to-day variability of the corresponding ENSO-related teleconnection pattern. Based on this, persistent

https://doi.org/10.5194/egusphere-2026-3344
Preprint. Discussion started: 14 July 2026

teleconnection pattern periods are defined when the daily pattern index exceeds 1.0 for at least 10 consecutive days. The 10-day persistence criterion follows previous studies of low-frequency circulation variability (Dole and Gordon, 1983; Li and Lau, 2012). To reduce boundary effects, this spatial projection-based identification is conducted over an extended SON season from 16 August to 15 December (121 days per year). The calendar distribution of identified pattern days during ENSO years is shown in Fig. 2, and the total number of EP El Niño-, CP El Niño-, and La Niña-related pattern days is 163, 204, and 289, respectively.

2.5 Cyclone day frequency under different sample spaces

Once the pattern periods are identified, all days within these periods are combined to form a conditional sample space representing the establishment of ENSO-related low-frequency teleconnection patterns in the extratropics. Before examining CDF under ENSO conditions, we first define the climatological CDF ($P(C)_{clim}$) as the probability of cyclone occurrence estimated over all extended SON days during the full period (1979-2022):

$$P(C)_{clim} = \frac{C_{all}}{TD_{all}} \times 100\% \quad (1)$$

where C_{all} denotes the number of cyclone-flagged days in all extended SON seasons, and TD_{all} denotes the total days of all extended SON seasons during 1979-2022 (121 days × 44 years = 5324 days).

To quantify ENSO-related changes under different sample spaces, CDF is computed within increasingly restricted subsets of extended SON days. First, under the conventional seasonal window, CDF during ENSO years is defined as:

$$P(C|ENSO) = \frac{C_{ENSO}}{TD_{ENSO}} \times 100\% \quad (2)$$

where C_{ENSO} denotes the number of cyclone-flagged days within extended SON seasons of ENSO years (for EP El Niño, CP El Niño, and La Niña years, respectively), and TD_{ENSO} denotes the corresponding total days of extended SON seasons of ENSO years (e.g., for EP El Niño, that is 121 days × 5 years = 605 days). Further, the CDF conditioned on the identified persistent pattern days ($P(C|ENSO, pattern)$) is defined as

$$P(C|ENSO, pattern) = \frac{C_{ENSO,pattern}}{TD_{ENSO,pattern}} \times 100\% \quad (3)$$

in which $C_{ENSO,pattern}$ denotes the counts of cyclone-flagged days in ENSO-related teleconnection pattern days, and $TD_{ENSO,pattern}$ denotes the total number of pattern days during corresponding ENSO years (e.g., for EP El Niño, that is 163 days in total). Actually, such a calculation can be interpreted as a conditional probability, which has also been used to quantify

https://doi.org/10.5194/egusphere-2026-3344
Preprint. Discussion started: 14 July 2026

the frequency changes in other weather systems (e.g., atmospheric blocking) associated with climate modes (Liu and Wang, 2024).

For comparison, CDF under the complementary non-pattern days within ENSO years is computed as:

$$P(C|ENSO, non-pattern) = \frac{C_{ENSO} - C_{ENSO,pattern}}{TD_{ENSO} - TD_{ENSO,pattern}} \times 100\% \quad (4)$$

The corresponding CDF anomalies under different sample spaces are calculated all relative to the climatological probability $P(C)_{clim}$. In addition to CDF, cyclone track density is calculated as the percentage of hours during which cyclone centres (SLP minima) are located within each 5° × 5° latitude-longitude grid cell over a given period (relative to the total hours in the sample space). Analogously, the track density is computed within the climatological, seasonal, pattern, and non-pattern sample spaces.

2.6 Significance test

The statistical significance of CDF anomalies associated with pattern and non-pattern days is assessed using a Monte Carlo resampling approach. For example, to evaluate the significance of $P(C|EP\ El\ Nino, pattern)$, a sample of 163 days (i.e. the total number of identified EP El Niño-related pattern days) is randomly drawn 1000 times from all extended SON days. For each resampling, CDF is calculated and the anomaly relative to $P(C)_{clim}$ is obtained. The resulting distribution of CDF anomalies represents the range under random resampling with the same sample size. If the observed anomaly of $P(C|EP\ El\ Nino, pattern)$ lies within the upper or lower 2.5% tails of the resample-based distribution, it is considered statistically significant at the 95% confidence interval. CDF significance associated with other conditions is evaluated through a similar procedure but using corresponding sample size for resampling.

For other regular variables (e.g., Z500 composites), statistical significance is assessed using a two-tailed Student's *t*-test (Wilks, 2011). To account for temporal autocorrelation in daily data, the effective degrees of freedom are estimated following Bretherton et al. (1999), and the *t*-test is adjusted accordingly.

2.7 Atmospheric dynamical diagnostics

Two atmospheric dynamical diagnostics are examined in this study, which are the upper-level Rossby wave source (RWS, at 200hPa) and lower-tropospheric baroclinicity (vertically averaged between 850-1000hPa). RWS is used to demonstrate the connection between tropical diabatic heating forcing and extratropical wave response, which is calculated following Sardeshmukh and Hoskins (1988), defined as $-\nabla \cdot (V_\chi \zeta)$, where V_χ is divergent wind vector and ζ the absolute vorticity. The baroclinicity is measured as Eady growth rate (EGR), which is a key parameter for extratropical cyclone activity with a

https://doi.org/10.5194/egusphere-2026-3344
Preprint. Discussion started: 14 July 2026

definition $\sigma_{BI} = 0.31f|\partial V_h/\partial z|/N$ (Lindzen and Farrell, 1980), where f is the Coriolis parameter, V_h is horizontal wind vector, and N is Brunt-Väisälä frequency.

https://doi.org/10.5194/egusphere-2026-3344
Preprint. Discussion started: 14 July 2026

3 Results

3.1 Persistent ENSO teleconnection pattern days: distribution and validation

First, we present seasonal patterns of tropical forcing and extratropical circulation responses during the extended SON season for different ENSO events (Fig. 1), which provide the large-scale background for the linkage between ENSO and synoptic weather systems. The SST anomalies (Fig. 1a-c) exhibit the spatial patterns of EP El Niño, CP El Niño, and La Niña events. Accompanying these SST patterns, EP El Niño is characterized by enhanced convection (negative OLR anomalies) extending from the central Pacific to east of the dateline, together with an east-west dipole across the tropical Indian Ocean (Fig. 1d). In comparison, CP El Niño shows weaker and westward-shifted convection anomalies (Fig. 1e), while La Niña basically displays an opposite pattern, with enhanced convection over the Maritime Continent and suppressed convection over the central Pacific (Fig. 1f). These distinct tropical convection anomalies drive different extratropical circulation responses. During EP El Niño, the 500-hPa geopotential height (Z500) anomalies exhibit a wave-train pattern with two branches, including a pronounced high-pressure anomaly south of Australia (Fig. 1g). For CP El Niño and La Niña, the PSA-like pattern dominates but with reversed polarity and discernible difference in spatial structure (Fig. 1g-i). Notably, the seasonal-mean circulation anomalies over Australia and the adjacent Tasman Sea (e.g. 20°S-40°S, 120°E-160°E) are much weaker than those over the South Pacific during CP El Niño and La Niña (Fig. 1h-i). This suggests that seasonal composites may not fully capture the regional signature within ENSO-related teleconnection patterns, motivating a focus on periods when these patterns are well established on daily timescale.

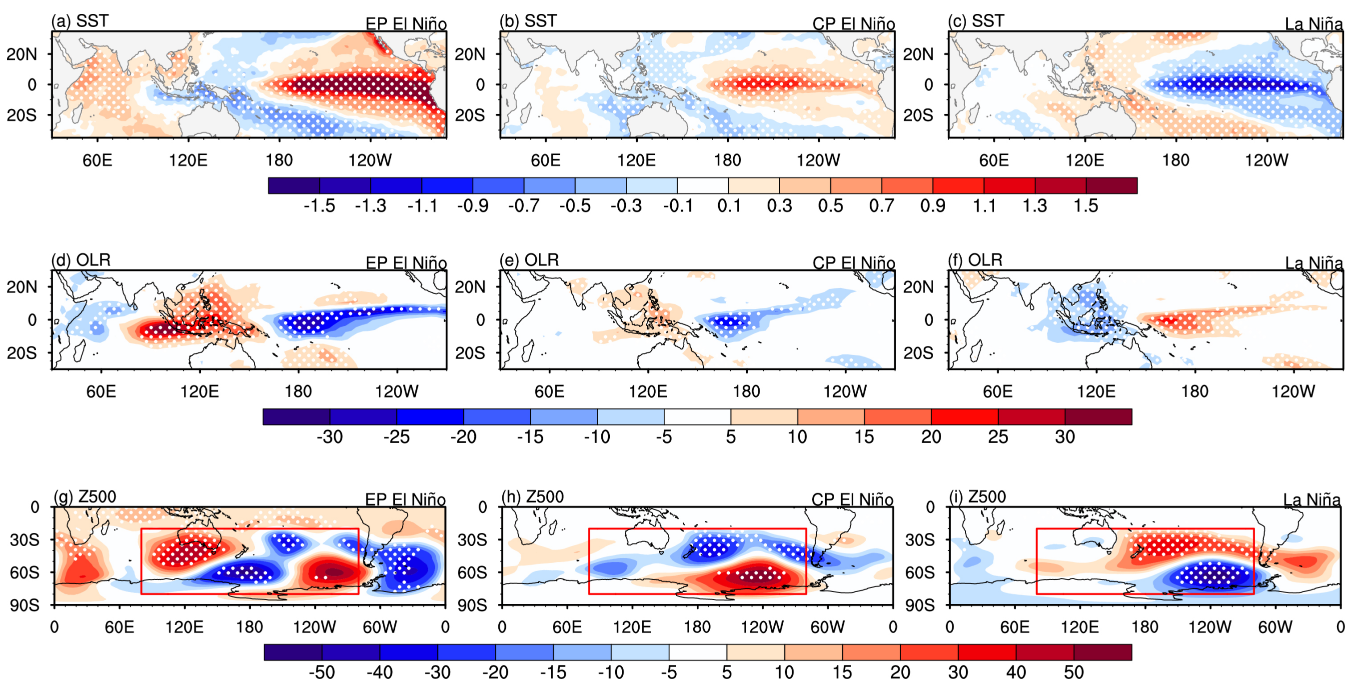

https://doi.org/10.5194/egusphere-2026-3344
Preprint. Discussion started: 14 July 2026

Figure 1. Composites of tropical convection and Southern Hemisphere circulation in SON season during ENSO events. (a-c) Sea surface temperature (SST; K), (d-f) outgoing longwave radiation (OLR; W/m^2), and (g-i) 500-hPa geopotential height (Z500; gpm) anomalies composited for EP El Niño (left), CP El Niño (middle), and La Niña (right) events. Stippling indicates regions where anomalies are statistically significant at the 95% confidence interval based on the two-tailed Student's *t*-test. Red boxes in (g-i) denote the domain used to define the reference patterns of extratropical teleconnection (20°S-80°S, 80°E-80°W) for spatial projection.

As ENSO-related teleconnection patterns are not continuously maintained throughout the season, we identify persistent periods exhibiting the teleconnection patterns associated with each ENSO type, following the approach described in Section 2.4. Their calendar distribution within the extended SON season is shown in Fig. 2. The identified pattern periods do not uniformly span the entire SON season but occur episodically, even with a degree of randomness in their timing. The total number of identified teleconnection pattern days is 163, 204, and 289 for EP El Niño, CP El Niño, and La Niña events, respectively. The inter-event differences are evident in the number and timing of identified pattern periods. Taking La Niña events as an example, more than 50 pattern days are identified in 1998 SON, whereas no pattern days are detected in 1999. In addition, although most ENSO years exhibit at least some corresponding pattern periods, there are years in which no pattern days are identified (e.g., 1983, 2007, and 2018), indicating that such low-frequency teleconnection patterns do not necessarily dominate on daily timescales in each ENSO year. These features suggest that even under the same ENSO phase, the extratropical teleconnection signal can be strongly influenced by atmospheric internal variability, leading to differences in the degree to which the teleconnection pattern is established. This further emphasizes the importance of focusing on the composites of teleconnection pattern days when detecting ENSO-related signals at daily timescales. Overall, these calendar distributions indicate that the seasonal-mean teleconnection signal might mainly arise from a limited number of persistent episodes, providing the basis for constructing a refined pattern-based sample space to examine cyclone statistics.

https://doi.org/10.5194/egusphere-2026-3344
Preprint. Discussion started: 14 July 2026

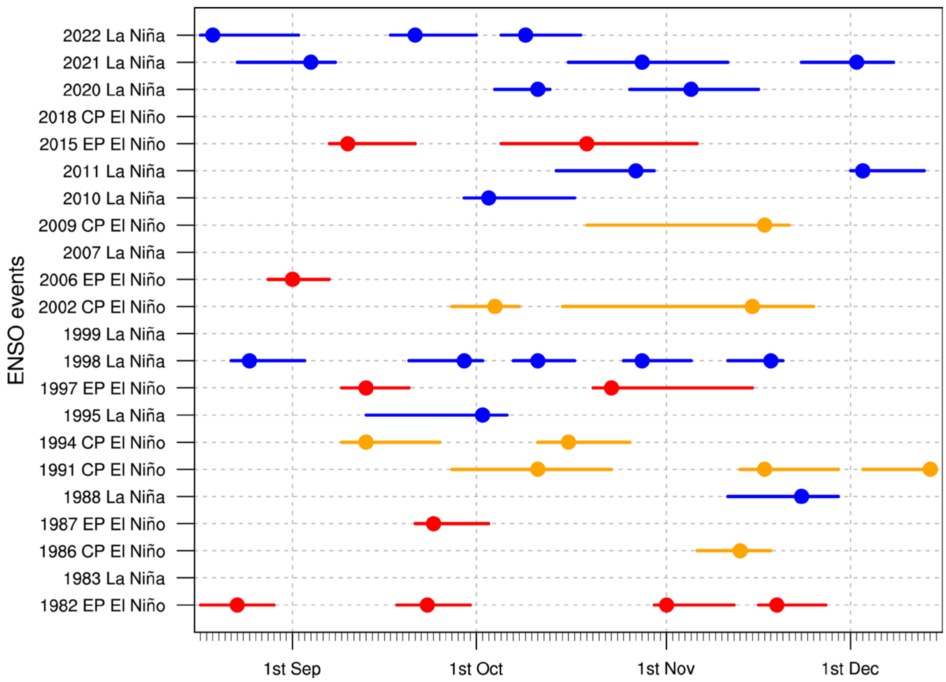

Figure 2. Temporal distribution of identified ENSO teleconnection pattern days during the extended SON season (16 August-15 December). Each line segment represents an identified pattern period, and the filled dot marks the day with the maximum projection index within that period. Colors denote ENSO types: EP El Niño (red), CP El Niño (yellow), and La Niña (blue).

Before examining cyclone statistics within the pattern-based sample space, it is necessary to validate the robustness of these identified pattern days to ensure that the subsequent conditioning is physically meaningful. So next, we check this issue from statistical and dynamical perspectives.

https://doi.org/10.5194/egusphere-2026-3344
Preprint. Discussion started: 14 July 2026

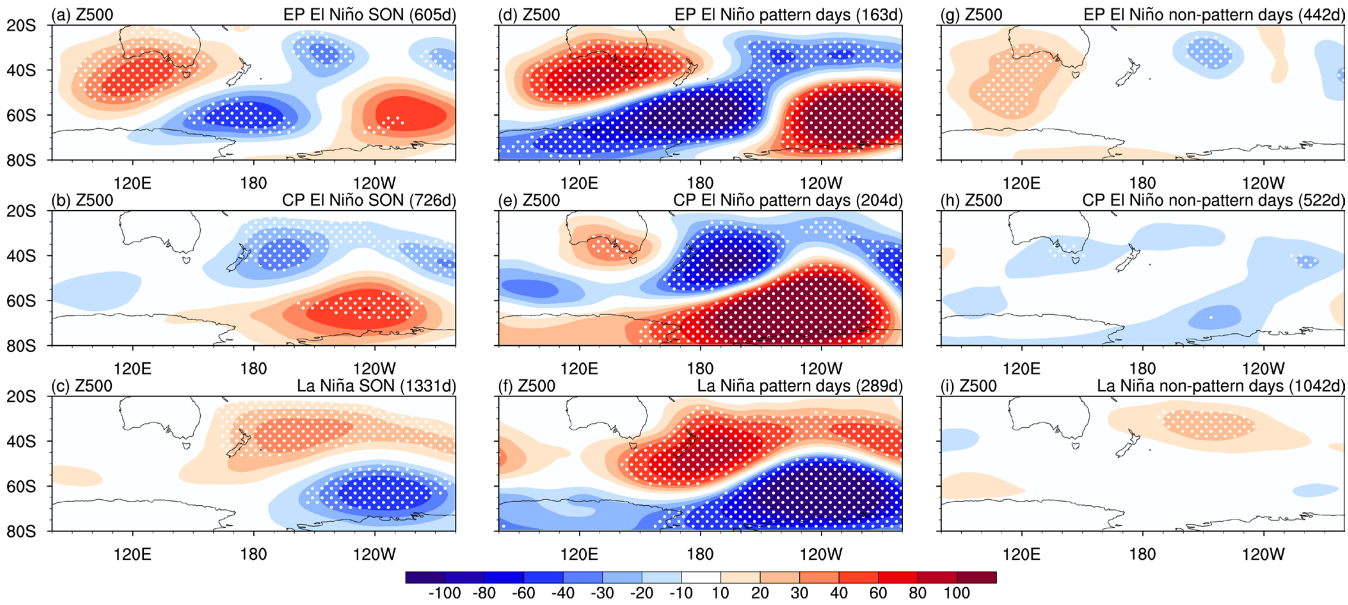

Figure 3. Comparison of circulation anomalies under different sample spaces during the extended SON season. Composited 500-hPa geopotential height anomalies (Z500; gpm) for all extended SON days (a-c), teleconnection pattern (d-f), and non-pattern (g-i) days under EP El Niño (top), CP El Niño (middle), and La Niña (bottom) years. The plotting area here is the same as the region outlined by the red box in Fig.1g-i. Stippling indicates regions where anomalies are statistically significant at the 95% confidence interval based on a two-tailed Student's *t*-test.

A first check is to compare the composited Z500 anomaly patterns based on all extended SON days (seasonal mean), the identified teleconnection pattern days, and the complementary non-pattern days (Fig. 3). It shows that the seasonal-mean ENSO teleconnection signal (Fig. 3a-c) primarily manifests in the pattern-day composites (Fig. 3d-f) in terms of spatial structure and anomaly amplitude. Specifically, for EP El Niño events, the pattern-day composite (Fig. 3d) captures the two-branch wave-train structure that is observed in the seasonal-mean field (Fig. 3a), including a pronounced high-pressure anomaly south of Australia and a PSA-like pattern mainly confined to the east of the dateline. For CP El Niño, the pattern-day composite exhibits a more pronounced PSA-like structure (Fig. 3e). Meanwhile a high-pressure anomaly south of Australia is also evident, suggesting that the daily establishment of the PSA-like pattern under CP El Niño is accompanied by a regional high-pressure signal in this area. For La Niña events, the atmospheric response exhibits a phase-reversed PSA-like pattern in both the seasonal-mean and pattern-day composite fields (Fig. 3c, f), while the latter shows a southwestward shifting of the high-pressure anomaly center and a broader influence over the Tasman Sea (Fig. 3f). In contrast, the composites based on non-pattern days show substantially weaker and patchy anomalies (Fig. 3g-i), particularly over the extratropics, suggesting that the extratropical response to ENSO is not continuously maintained throughout the season and could be affected by atmospheric internal variability. Therefore, these results confirm that when examining the extratropical ENSO-related variability on daily

https://doi.org/10.5194/egusphere-2026-3344
Preprint. Discussion started: 14 July 2026

timescale, it is necessary to focus on periods during which the teleconnection patterns are fully established to better capture the ENSO-related signal.

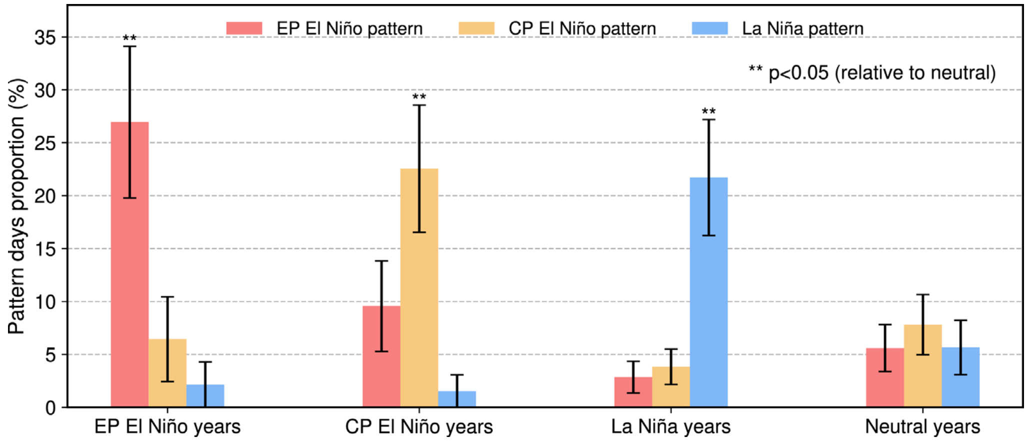

Figure 4. Proportion of identified teleconnection pattern days relative to the total days in the extended SON season under different years. For each teleconnection pattern (EP El Niño, CP El Niño, and La Niña patterns), pattern days are identified annually using the same projection method as described in Section 2.4, and the proportion of pattern days relative to extended SON season (121 days) is calculated. Bars show the mean proportion averaged under EP El Niño years, CP El Niño years, La Niña years, and neutral years, respectively. Error bars denote the standard deviation of the proportions within each category. Double asterisks indicate that the mean proportion differs significantly from that of neutral years at the 95% confidence interval based on a one-tailed Student's *t*-test.

We further check the proportion of teleconnection pattern days relative to the total days in the extended SON season under different years. It clearly shows that each specific teleconnection pattern occurs more frequently during the corresponding ENSO years (Fig. 4). Moreover, the proportions of EP El Niño, CP El Niño, and La Niña pattern days are all significantly higher during their respective ENSO years than during neutral years. These ENSO-dependent differences indicate that the systematic occurrence of identified persistent pattern days is modulated by corresponding ENSO events, rather than arising solely from internal atmospheric variability.

At the end of this section, we conduct a cross-validation on the identified teleconnection pattern days from a dynamical perspective. It's well known that ENSO-related extratropical teleconnections are generally interpreted as a result of Rossby wave propagation triggered by anomalous tropical diabatic heating associated with ENSO events. Therefore, a coherent lead-lag relationship between tropical convection anomalies and extratropical circulation response could be expected on daily timescales (Franzke et al., 2011; Stan et al., 2017).

https://doi.org/10.5194/egusphere-2026-3344
Preprint. Discussion started: 14 July 2026

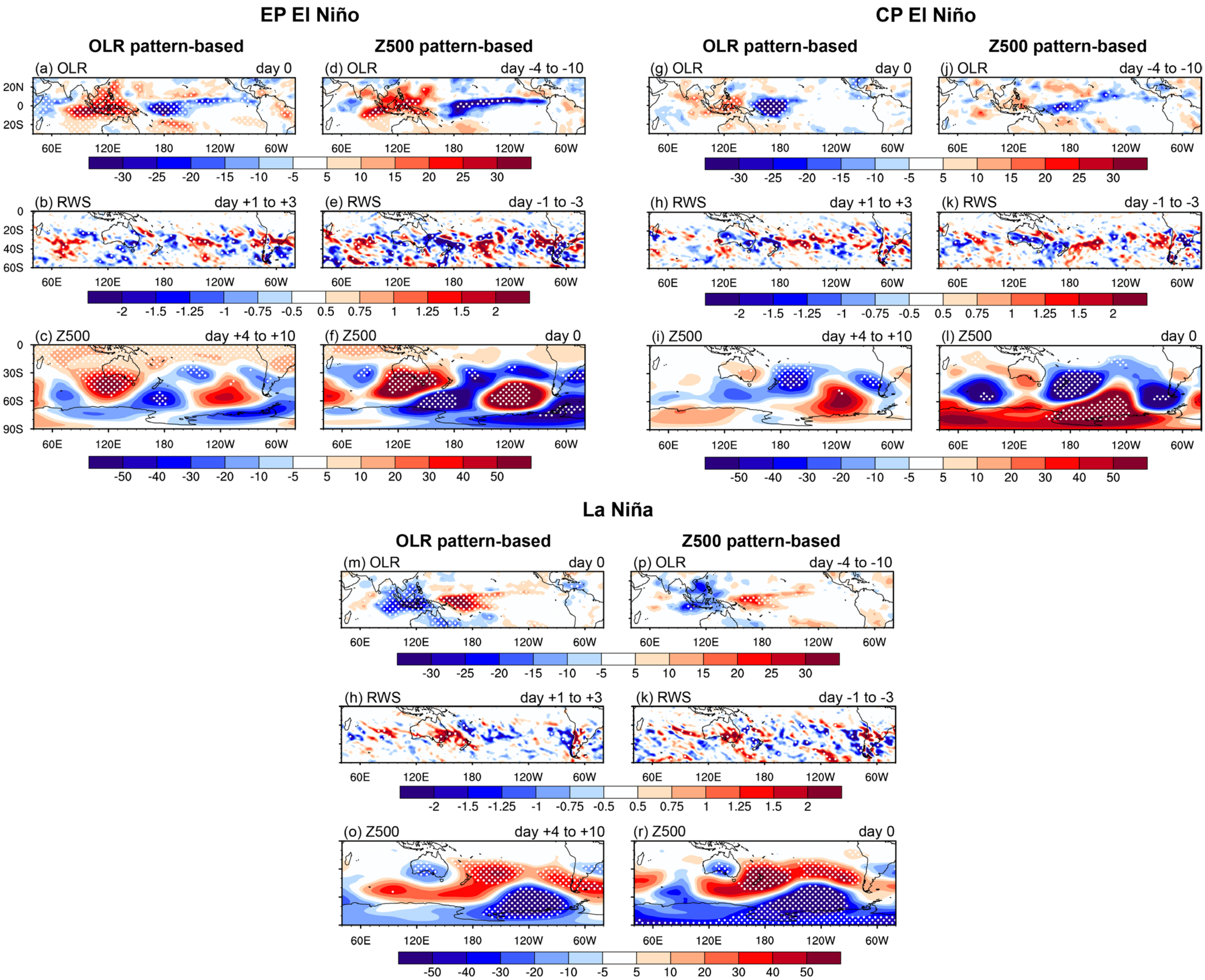

Figure 5. Cross-validation using the lead-lag composite based on OLR and Z500 pattern identification. For each ENSO type (EP El Niño, CP El Niño, and La Niña), the left column shows composites based on OLR-pattern events, and the right column shows composites based on Z500-pattern events. For the OLR pattern-based (a-c, g-i, and m-o), day 0 denotes the first day of OLR pattern events, the top panel (a, g, m; units: W/m^2) shows composited OLR anomalies on day 0, the middle panel (b, h, n; units: $10^{-10}s^{-2}$) shows 200hPa RWS anomalies averaged over days +1 to +3, and the bottom panel (c, i, o; units: gpm) shows Z500 anomalies averaged over days +4 to +10. For the Z500 pattern-based (d-f, j-l, and p-r), day 0 denotes the day with maximum projection index in each Z500 pattern period (see the filled dots in Fig. 2), the bottom panel (f, l, r) shows composited Z500 anomalies on day 0, the middle panel (e, k, q) shows RWS anomalies averaged over days -1 to -3, and the top panel (d, j, p) shows OLR anomalies averaged over days -4 to -10. Stippling indicates regions where anomalies are statistically significant at the 95% confidence interval based on two-tailed Student's *t*-test.

https://doi.org/10.5194/egusphere-2026-3344
Preprint. Discussion started: 14 July 2026

Following this idea, we also identify OLR pattern days by applying a similar spatial projection-based method on the daily OLR anomaly fields, but using ENSO-composited SON mean OLR anomalies over the tropical Indo-Pacific region (10°S-10°N, 80°E-150°W) as the reference pattern (Fig.1d-f). Considering the more transient nature of tropical convection (Branstator, 2014), a threshold of 1.5 standard deviations and a persistence criterion of 3 consecutive days are applied to define OLR pattern events. Sensitivity tests indicate that slightly changing the thresholds does not largely affect the results. Taking the initial day of each OLR pattern event as day 0, we conduct OLR-pattern-based composites by examining OLR anomalies at day 0, anomalous 200hPa RWS averaged over days +1 to +3, and lagged Z500 anomalies averaged over days +4 to +10. Correspondingly, for Z500-pattern-based composites, we define day 0 as the day with the maximum daily pattern index in each Z500 pattern event. In this case, we composite the days prior to the extratropical response to detect the tropical forcing. Specifically, we examine Z500 anomalies at day 0, RWS anomalies averaged over days -1 to -3, and preceding OLR anomalies averaged over days -4 to -10. This procedure is applied separately to EP El Niño, CP El Niño, and La Niña events (Fig. 5). Overall, the results show that, whether starting from OLR-pattern-based composites to examine the lagged response (Fig. 5a-c, g-i, and m-o) or from Z500-pattern-based composites to examine the preceding forcing source (Fig. 5d-f, j-l, and p-r), the composited anomaly fields of the same variable exhibit similar spatial structures under the corresponding ENSO types. These similarities are further supported by spatial pattern correlations, all of which exceed the 95% confidence interval of the bootstrap resampling-based significance test (Table 2). It is worth noting that although RWS correlations are relatively low, likely due to the intrinsic noisy nature of daily RWS fields, they remain statistically significant according to the bootstrap test. Therefore, such consistency further supports the robustness of identified Z500-based pattern days from the perspective of ENSO teleconnection dynamics, providing a physically grounded basis for using these periods as the sample space for detecting changes in cyclone statistics.

https://doi.org/10.5194/egusphere-2026-3344
Preprint. Discussion started: 14 July 2026

Table 2. Spatial pattern correlations of anomaly fields between Z500- and OLR-based composites (Fig. 5) for different ENSO types. The latitude-longitude range shown in parentheses indicates the spatial domain over which the correlations are calculated for each variable. Statistical significance is assessed using a bootstrap resampling approach. For each ENSO type, the Z500-pattern-based composites are fixed (i.e., the right columns for each ENSO type in Fig. 5), while random composites are generated by resampling the same number of days as used in the corresponding OLR-pattern-based composites before. The spatial correlation between the fixed Z500-based composite and random composite is calculated, and this procedure is repeated 1000 times to obtain a bootstrap distribution of spatial correlations. The range in square brackets denotes the 95% bootstrap confidence intervals (CI). Asterisks indicate that the correlations exceed the 95% bootstrap CI thus can be regarded as statistically significant.

Anomaly fields	EP El Niño	CP El Niño	La Niña
OLR (10°S-10°N, 80°E-150°W)	0.87* [-0.15, 0.75]	0.74* [-0.29, 0.69]	0.92* [-0.73, 0.36]
RWS (20°S-40°S, 60°E-100°W)	0.18* [-0.19, 0.13]	0.32* [-0.15, 0.24]	0.22* [-0.16, 0.18]
Z500 (20°S-80°S, 80°E-80°W)	0.84* [-0.39, 0.75]	0.57* [-0.69, 0.36]	0.81* [-0.38, 0.72]

3.2 Changes in cyclone statistics conditioned on teleconnection pattern days

In this section, we present the changes in cyclone statistics under ENSO teleconnection pattern conditions. Before examining these changes, we first show the climatology of cyclone day frequency and cyclone track density during the SON season in the Southern Hemisphere for the period 1979-2022 (Fig. 6). Although the two metrics are defined differently, they both represent the spatial distribution of cyclone activity. For extratropical cyclones, their highest activity zone coincides with the well-known storm track over the Southern Ocean, together with a secondary region of relatively frequent occurrence over the Tasman Sea. These climatological distributions provide a reference state for examining ENSO-related changes. However, it should be noted that some hot spots with large values over the tropical land, such as southern Africa, northwestern Australia, and parts of South America, actually reflect shallow heat lows that are also detected by the SLP-based identification scheme and are not the focus of this study.

https://doi.org/10.5194/egusphere-2026-3344
Preprint. Discussion started: 14 July 2026

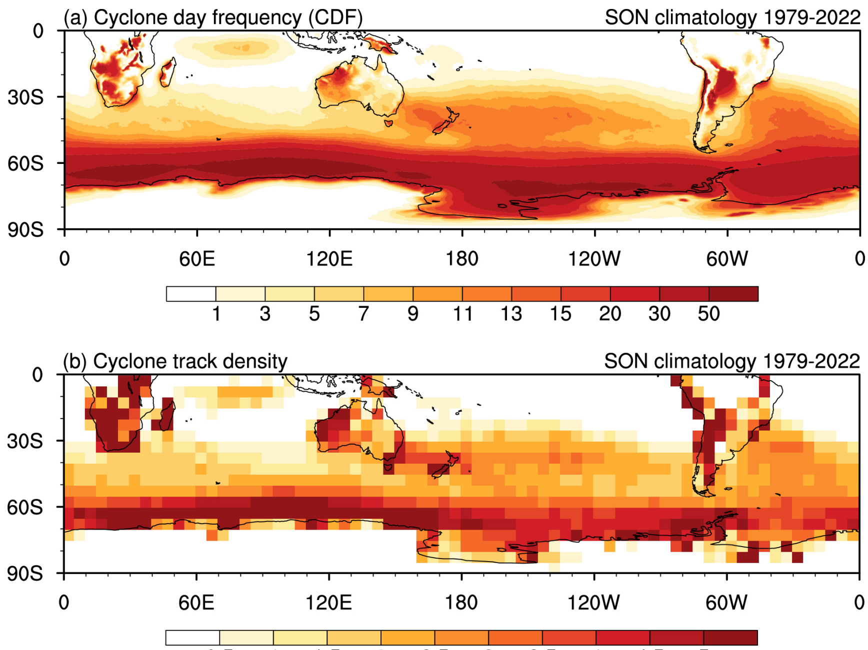

Figure 6. Climatological distribution of (a) cyclone day frequency (units: %) and (b) cyclone track density (units: counts per 100 hours per 5°×5° grid box) in the Southern Hemisphere during the extended SON season for the period 1979-2022.

3.2.1 Comparison among different sample spaces

Now we present CDF anomalies calculated using the conventional seasonal window, ENSO-related pattern days, and non-pattern days (Fig. 7). Comparing these results across the three different sample spaces can provide a clear view of how the pattern-based conditioning helps capture the response of cyclone activity to ENSO events.

First, the results based on the conventional seasonal window (Fig. 7a-c) serve as a baseline for the comparison here. In the extratropical Australian region, both over land and the adjacent ocean, the anomalies are generally weak or nearly absent, particularly for CP El Niño and La Niña. This absence of significant CDF anomalies around Australia agrees with the statements from previous studies that suggest overall no clear link between ENSO and Australian extratropical cyclones (Grosfeld et al., 2021; Pepler et al., 2014b). Nevertheless, in the storm-track region, especially over the mid- to high-latitude South Pacific, coherent large-scale anomaly patterns are evident. These patterns are physically consistent with the seasonal Z500 anomalies (Fig. 1g-i), characterized by increased (decreased) CDF accompanying negative (positive) geopotential height anomalies. Such consistency between changes in synoptic-scale cyclone activity and seasonal-mean circulation essentially reflects the dynamic nature of transient eddy-mean flow interaction inherent in the extratropical atmosphere. However, when focusing on the pattern-based sample space (Fig. 7d-f), CDF anomaly signals become more pronounced, both in magnitude and in the spatial extent of statistically significant regions. Importantly, the large-scale anomaly patterns remain consistent

https://doi.org/10.5194/egusphere-2026-3344
Preprint. Discussion started: 14 July 2026

with those obtained from the conventional seasonal window (Fig. 7a-c), while additional regional signals emerge under pattern-day conditions. In particular, around the extratropical Australia, significant CDF anomalies emerge over the Tasman Sea (region indicated by black box), where cyclone day frequency increases (decreases) by up to approximately 10% relative to climatology during La Niña (El Niño) (Fig. 7d-f). These suggest that conditioning on pattern days does not alter the basic large-scale structure of ENSO-related cyclone responses, which is constrained by the associated atmospheric teleconnections, but enhances the detectability of significant anomalies of cyclone activity by improving the signal-to-noise ratio. In contrast, CDF anomalies calculated from non-pattern days are much weaker and exhibit a patchy spatial distribution (Fig. 7g-i), demonstrating from a contrasting side that the ENSO-related signal of cyclone statistics change is more feasibly detected under the identified pattern days.

Similarly, we also check the corresponding changes in cyclone track density under different sample spaces (Fig. S2). Although the anomaly fields appear blocky due to the definition of track density, the large-scale spatial patterns obtained under pattern-day conditions (Fig. S2d-f) are generally consistent with the CDF results (Fig. 7d-f), further supporting the above findings. Together, these results provide clear evidence for the modulation of ENSO teleconnection patterns on extratropical cyclone activity.

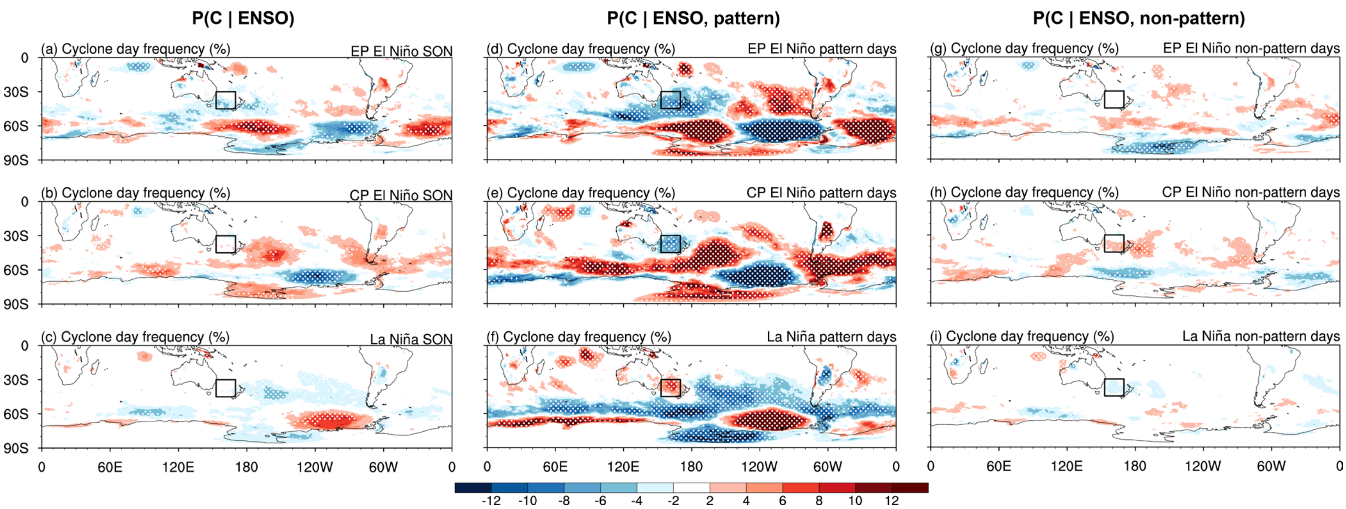

Figure 7. Cyclone day frequency anomalies under different sample spaces during ENSO events. Columns show the anomaly field of CDF (%) calculated based on (a-c) all the extended SON-season days, (d-f) ENSO-related teleconnection pattern days, and (g-i) non-pattern days. Rows correspond to EP El Niño (top), CP El Niño (middle), and La Niña (bottom) events. Stippling indicates regions where anomalies are statistically significant at the 95% confidence interval based on Monte Carlo resampling test. The black box outlines the Tasman Sea region (30°S-45°S, 153°E-170°E).

Considering that the atmospheric baroclinicity is a key control of extratropical cyclones, many of which are essentially unstable baroclinic eddies in midlatitude westerly flow, we further examine whether baroclinicity anomalies are consistent with the

https://doi.org/10.5194/egusphere-2026-3344
Preprint. Discussion started: 14 July 2026

cyclone changes in the Southern Hemisphere extratropics. To this end, we composite anomalies of Eady growth rate under different sample spaces (Fig. 8).

Still starting from the extended SON seasonal mean results (Fig. 8a-c), distinct EGR anomaly patterns are evident among the three ENSO types. EP El Niño is characterized by a zonally wave-like structure, while CP El Niño and La Niña exhibit relatively uniform negative and positive anomalies, respectively, confined over the midlatitude South Pacific. Comparing with the corresponding CDF anomalies (Fig. 7a-c), positive (negative) EGR anomalies are generally associated with enhanced (suppressed) cyclone frequency on their poleward flank and downstream region. This feature is consistent with the downstream development and poleward movement of baroclinic eddies in the storm tracks (Simmons and Hoskins, 1979; Thorncroft et al., 1993). The EGR anomalies become much more pronounced when composited over ENSO-related pattern days (Fig. 8d-f). They maintain similar large-scale spatial patterns to those in the seasonal mean composites (Fig. 8a-c) but exhibit substantially enhanced magnitude, particularly over the Southern Ocean south of 40°S. These EGR anomaly patterns are also in agreement with the distribution of CDF anomalies under pattern-day conditioning (Fig. 7d-f). It is worth noting that over the Tasman Sea region, where significant CDF anomalies emerge under pattern days, the corresponding EGR anomalies are relatively weak (Fig. 8d-f). This subtle fact implies that cyclones active in this region may differ from midlatitude baroclinic eddies, their activity is more possibly influenced by localized dynamical and thermodynamical factors. In contrast, the EGR anomalies composited under non-pattern days are quite weak and spatially patchy, indicating that ENSO-related baroclinicity anomalies are also concentrated in the identified pattern days. Overall, the consistency between baroclinicity anomalies and cyclone frequency changes further supports that ENSO teleconnection patterns modulate the large-scale structure of extratropical cyclone activity through affecting the midlatitude baroclinicity.

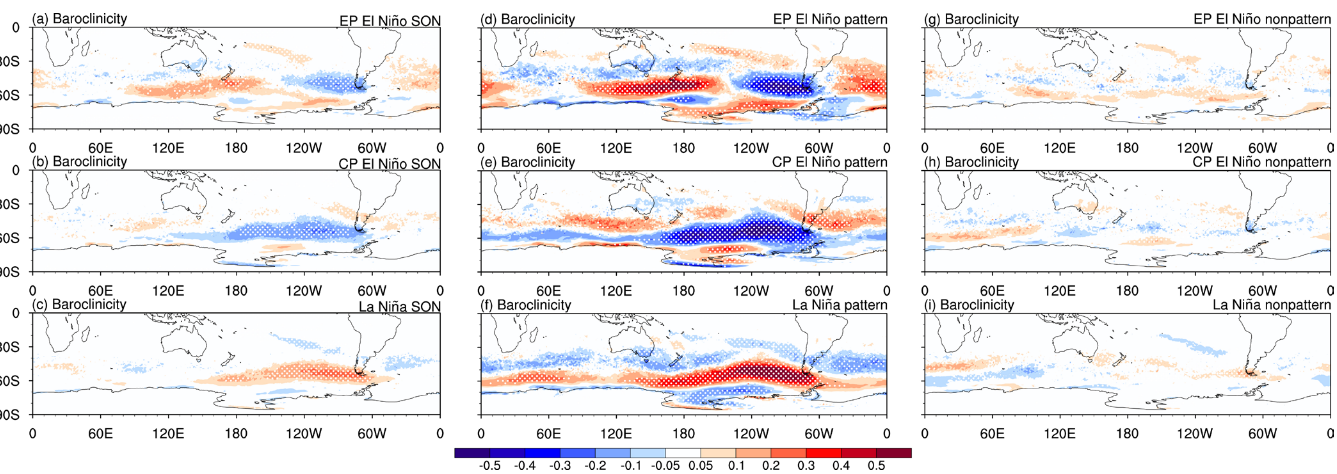

Figure 8. Composited low-level atmospheric baroclinicity anomaly (1000-850hPa vertically averaged Eady growth rate; day^{-1}) during the extended SON season (a-c), teleconnection pattern days (d-f), and non-pattern days (g-i) for the EP El Niño (top), CP El Niño (middle), and La Niña (bottom) events. Stippling indicates regions where anomalies are statistically significant at the 95% confidence interval based on two-tailed Student's *t*-test.

https://doi.org/10.5194/egusphere-2026-3344
Preprint. Discussion started: 14 July 2026

3.2.2 Tasman Sea cyclone changes and associated environmental factors

As a key region where synoptic systems exert important impacts on southeastern Australian weather, the Tasman Sea becomes an area of particular interest due to the significant CDF anomalies identified under ENSO-related pattern days (Fig. 7d-f). Therefore, we further examine Lagrangian metrics of the cyclones passing through this region, including tracks, local genesis frequency, residence time, and intensity.

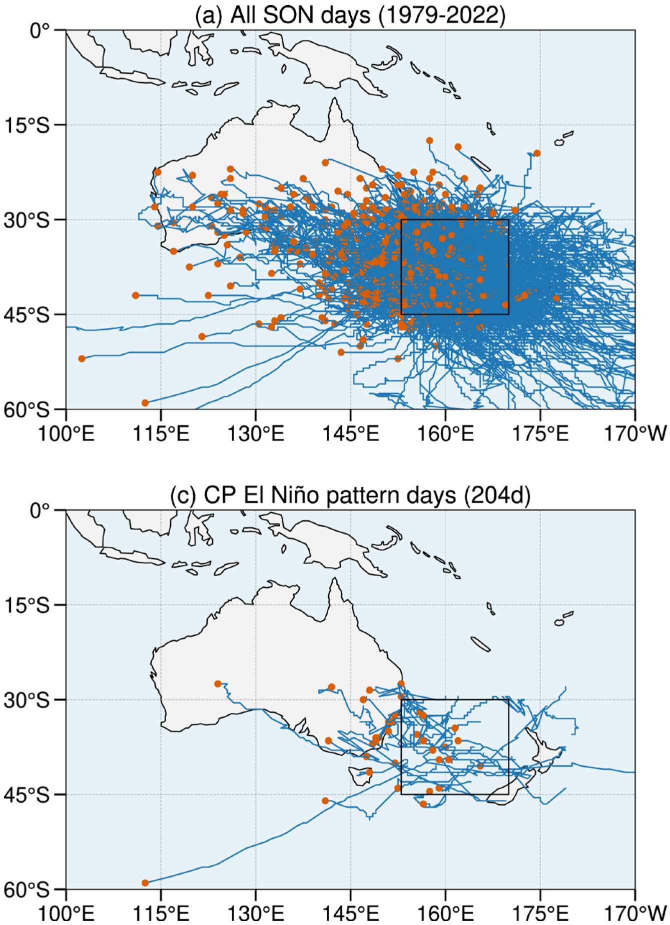

Figure 9. Cyclone tracks passing through the Tasman Sea during (a) the extended SON season for all years (1979-2022), (b) EP El Niño pattern days, (c) CP El Niño pattern days, and (d) La Niña pattern days. Cyclones are considered as passing through the Tasman Sea if their lifetime exceeds 12 hours and at least 10% of their track points are located within the Tasman Sea region. Blue lines denote individual cyclone tracks, and orange dots indicate cyclogenesis locations (initial points of tracks). The black box outlines the Tasman Sea region (30°S-45°S, 153°E-170°E).

We first show the tracks of cyclones passing through the Tasman Sea (box outlined in Figs. 7 and 9; 30°S-45°S, 153°E-170°E) for all extended SON days during 1979-2022, as well as for EP El Niño pattern days (163 days), CP El Niño pattern days (204 days), and La Niña pattern days (289 days), respectively (Fig. 9). Given the different sample sizes, the tracks shown in the

https://doi.org/10.5194/egusphere-2026-3344
Preprint. Discussion started: 14 July 2026

maps may not be directly comparable in terms of distribution density but instead are used to illustrate structural differences in cyclone pathways and genesis locations. The tracks for all extended SON days (1979-2022) indicate that cyclones passing through the Tasman Sea are predominantly generated locally or originate from nearby tropical and subtropical areas, with relatively few systems propagating remotely from upstream storm tracks as midlatitude baroclinic eddies (Fig. 9a). This suggests that cyclone activity over the Tasman Sea might be substantially attributed to local subtropical systems, whose development depends not only on baroclinic instability but also strongly on localized diabatic heating and dynamical conditions (Pepler et al., 2016). This in turn provides a plausible explanation for why the EGR anomalies in the Tasman Sea region under ENSO-related pattern days do not align well with the corresponding regional CDF anomalies (Fig. 7d-f and Fig. 8d-f). Despite the differences in sample sizes, compared with La Niña conditions (Fig. 9d), it seems that very few cyclones during El Niño originate or propagate from the tropical ocean east of Australia (north of 30°S) into the Tasman Sea (Fig. 9b-c). This indicates a potential suppression of cyclone genesis and movement from the tropics into the Tasman Sea during El Niño, which is likely associated with some unfavourable environmental conditions for cyclone development.

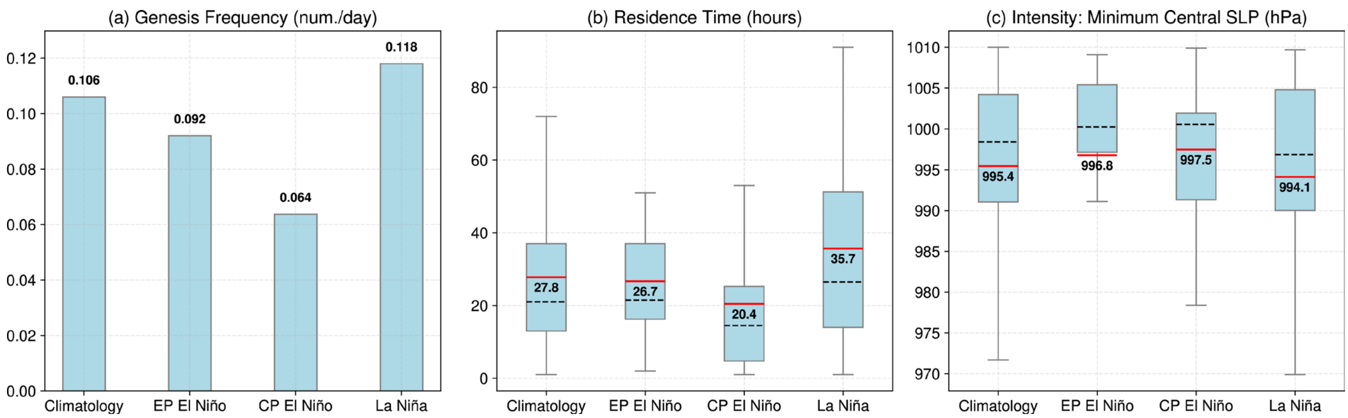

Figure 10. Statistical characteristics of cyclones passing through the Tasman Sea during the extended SON season for all years (climatology), EP El Niño pattern days, CP El Niño pattern days, and La Niña pattern days. (a) Genesis frequency (number per day) of cyclones originating within the Tasman Sea region. (b) Residence time (hours) of cyclones over the Tasman Sea region. (c) Cyclone intensity measured by the minimum central SLP (hPa) of cyclones during passing through the Tasman Sea. In (b) and (c), box plots show the interquartile range, with the red solid line indicating the mean and the dashed line indicating the median; whiskers denote the full range of the data.

We further calculate the statistics of individual cyclones focusing on their genesis location and residence period over the Tasman Sea (Fig. 10). Specifically, the genesis frequency (Fig. 10a) is defined as the ratio of the number of cyclones generated over the Tasman Sea to the total number of days in the corresponding sample space (including all extended SON days during 1979-2022 as the climatology, as well as EP El Niño, CP El Niño, and La Niña pattern days). The residence time (Fig. 10b) is defined as the average duration (in hours) that cyclone tracks remain within the Tasman Sea region, and the intensity (Fig. 10c) is represented by the minimum central pressure of cyclones while passing through the region. The genesis frequency decreases under El Niño pattern days relative to the climatological value, particularly for CP El Niño, whereas it shows an increase under

https://doi.org/10.5194/egusphere-2026-3344
Preprint. Discussion started: 14 July 2026

La Niña conditions (Fig. 10a). For the residence time, an increase is evident during La Niña pattern days, while a modest decrease is observed during El Niño pattern days (Fig. 10b). Together, these provide an interpretation of the CDF anomalies identified over the Tasman Sea (Fig. 7d-f), indicating that they are associated with changes in local cyclogenesis and residence time under ENSO-related pattern conditions. By comparison, changes in cyclone intensity are relatively not obvious (Fig. 10c). Apart from a slight weakening under EP El Niño, there seems to be no significant and systematic change whether under CP El Niño or La Niña, which reflects the difficulty in directly linking intensity changes of individual extratropical cyclones to remote climate drivers within such a cross-scale context.

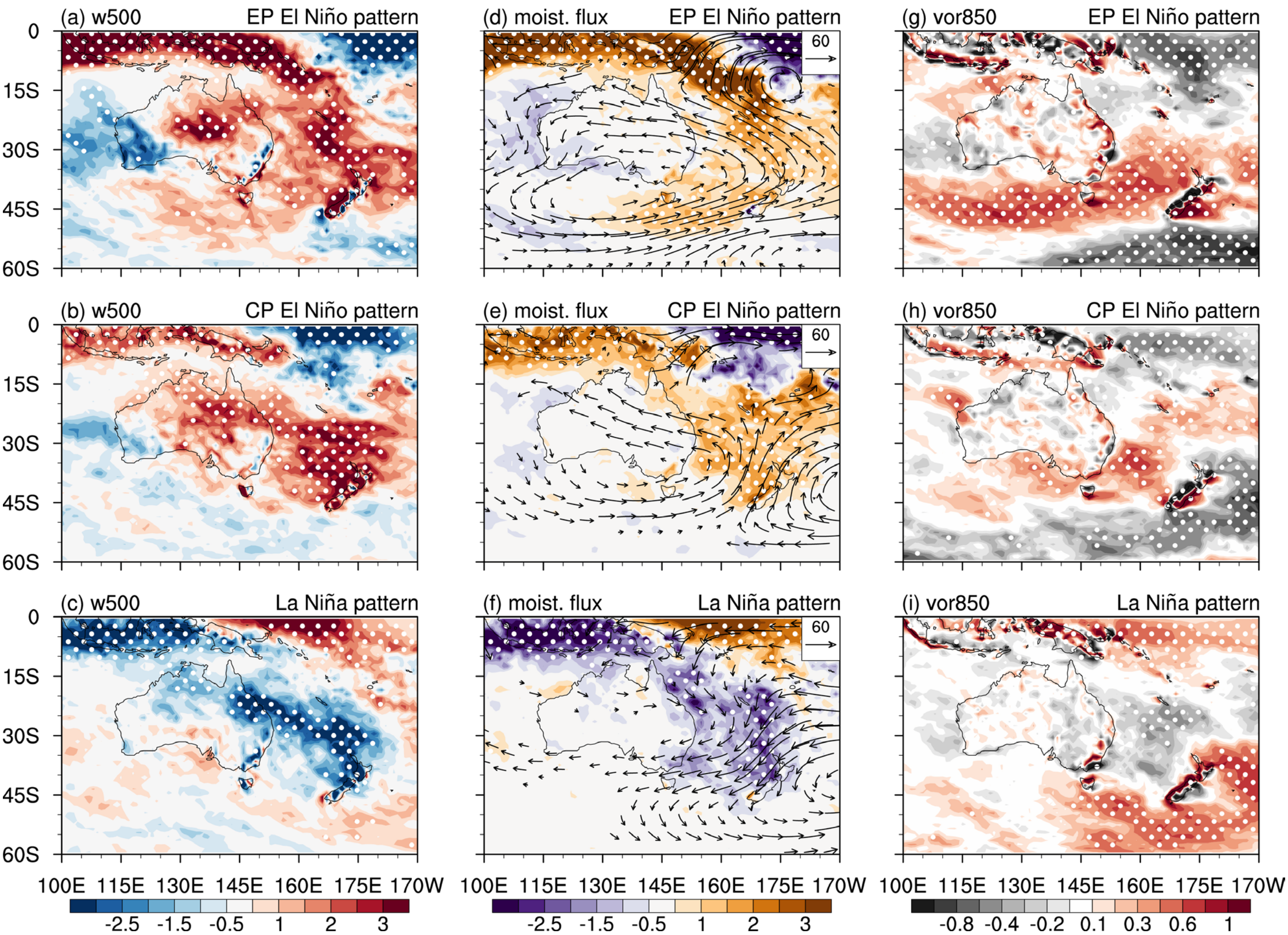

Figure 11. Pattern-days composites of environmental factors around Australia. Composited anomalies of vertical velocity at 500hPa (a-c; 10^{-2}Pa/s), vertically integrated moisture flux (d-f; vectors; kg/m/s) with moisture flux divergence (shading; 10^{-5}kg/m^2/s), and relative vorticity at 850hPa (g-i; s^{-1}) during EP El Niño pattern days (top), CP El Niño pattern days (middle), and La Niña pattern days (bottom). Stippling indicates regions where anomalies are statistically significant at the 95% confidence interval based on two-tailed Student's *t*-test.

The above analysis reveals the changes in Tasman Sea cyclone statistics modulated by different ENSO-related teleconnection patterns. We further examine the associated environmental factors that are closely related to local cyclone development. Here we construct composites over pattern days for 500-hPa vertical velocity, vertically integrated moisture flux and its divergence, and 850-hPa relative vorticity (Fig. 11). Under El Niño-related pattern days, both EP and CP types exhibit anomalously suppressed ascent (Fig. 11a-b) and moisture divergence (Fig. 11d-e) over the Tasman Sea, thus unfavourable for cyclone activity here. In addition, these unfavourable conditions extend northward along the eastern Australian coast into the tropical ocean and then might suppress the genesis of tropical cyclones in this upstream region, which is relevant to the earlier observation that cyclone tracks originating from tropics to the Tasman Sea seems reduced under El Niño conditions (Fig. 9b-c). In contrast, under La Niña pattern days, enhanced ascent (Fig. 11c) and moisture convergence (Fig. 11f) are evident over the Tasman Sea, providing a more favourable environment for increased cyclone activity. The anomalous anticyclonic high-pressure system downstream (Fig. 3f) and associated warm-moist air transport by the anomalous northeasterly flow from the tropics (Fig. 11f), are consistent with the typical synoptic weather type linking Australian east coast lows (cutoff lows) with atmospheric blockings, as documented in previous studies (Cowan et al., 2013; Gillett et al., 2023; Holgate et al., 2022). As another key variable associated with cyclone activity, low-level relative vorticity exhibits anticyclonic, positive (cyclonic, negative) anomalies over the Tasman Sea under El Niño (La Niña) pattern days (Fig. 11g-i), which are dynamically consistent with the corresponding changes in cyclone frequency there. Overall, these changes in environmental factors help us provide a physical explanation for the observed CDF anomalies under the pattern-day conditioning, suggesting that ENSO teleconnections modulate Tasman Sea cyclone activity through their influence on local dynamical and moisture processes.

3.3 Eastern Australian rainfall anomalies associated with Tasman Sea cyclone changes

Since we have shown that ENSO teleconnection patterns modulate cyclone activity over the Tasman Sea, it is of interest to explore to what extent these cyclone changes affect Australian rainfall, particularly for eastern Australia. We still start by comparing rainfall anomalies composited over the extended SON season, pattern days, and non-pattern days of ENSO years (Fig. 12). For the seasonal composites (Fig. 12a-c), the Australian spring rainfall anomalies exhibit the well-known anomalous dry (wet) feature during El Niño (La Niña). There are also moderate differences associated with ENSO diversity. In EP El Niño, significant negative anomalies are concentrated over the Northern Territory, the southeastern Murray-Darling Basin, and parts of southwestern Australia (Fig. 12a). CP El Niño and La Niña show significant anomalies concentrated over eastern Australia, while with stronger positive rainfall anomalies during La Niña (Fig. 12c), consistent with our recent study of diverse ENSO impacts on Australian spring rainfall (Sun et al., 2026). When focusing on the pattern days (Fig. 12d-f), the composited rainfall anomalies exhibit consistent spatial patterns with the seasonal-mean results but manifest stronger magnitude. In contrast, the anomalies associated with non-pattern days are relatively weaker (Fig. 12g-i). Therefore, similar to the results for Z500 (Fig. 3) and EGR (Fig. 8), this indicates that ENSO-related rainfall signals, particularly over the southeastern Australia, are also primarily associated with rainfall variability during the corresponding teleconnection pattern days, thus motivating a

https://doi.org/10.5194/egusphere-2026-3344
Preprint. Discussion started: 14 July 2026

further investigation on eastern Australian rainfall anomalies within pattern days (Fig. 12d-f) and exploring their relationship with cyclone changes over the Tasman Sea.

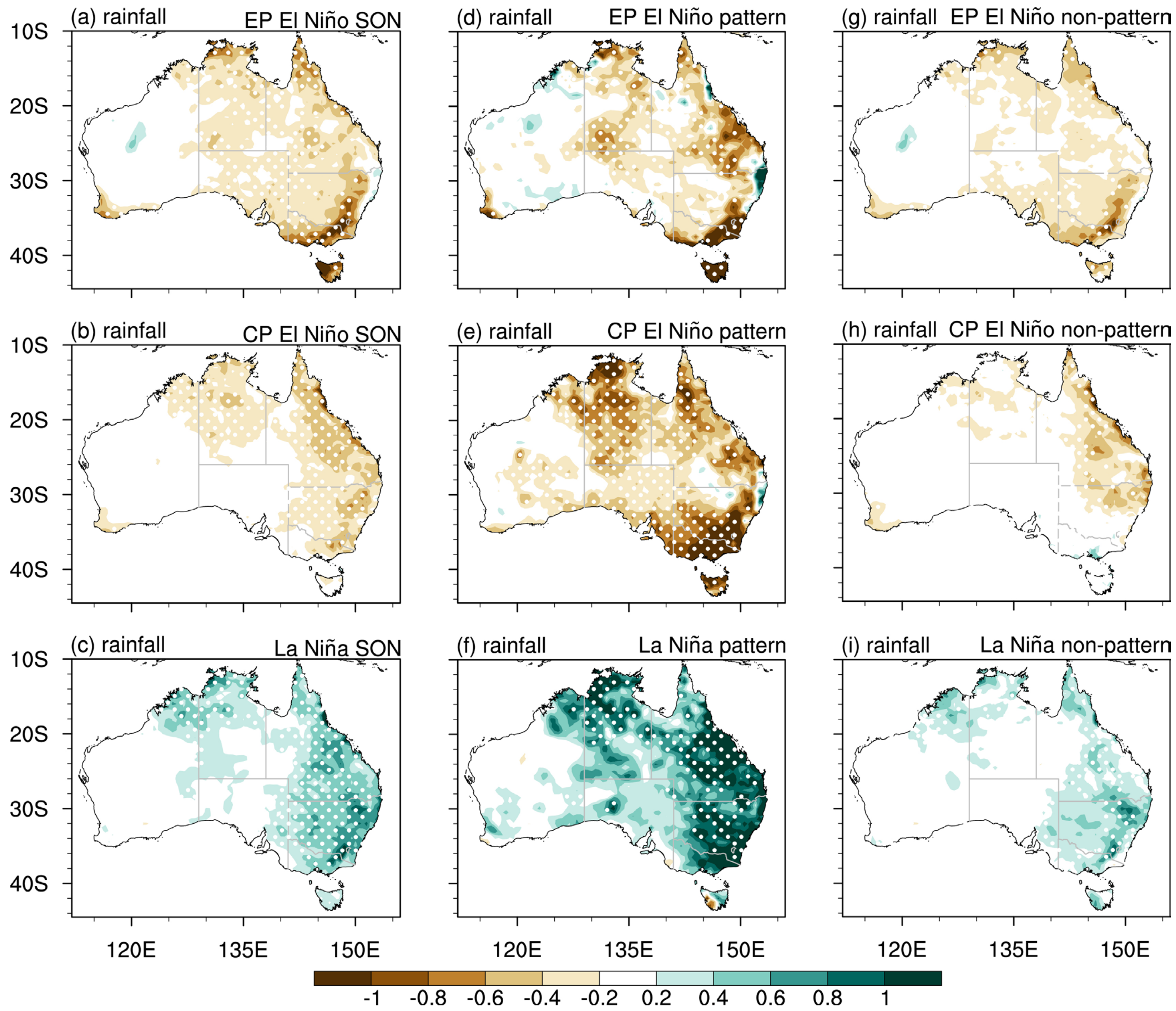

Figure 12. The Australian rainfall anomalies (units: mm/day) composited over the whole extended SON days (a-c), pattern days (d-f), and non-pattern days (g-i) under the EP El Nino (top), CP El Nino (middle), and La Nina events (bottom). The white stippling indicates regions where anomalies are statistically significant at the 95% confidence interval based on two-tailed Student's *t*-test.

Here it should be emphasized that, because of different sample sizes, our focus is not on the total precipitation, but on mean rainfall anomalies in eastern Australia associated with changes of Tasman Sea cyclone activity during ENSO-related pattern

https://doi.org/10.5194/egusphere-2026-3344
Preprint. Discussion started: 14 July 2026

days. To achieve this, we first propose a general classification of cyclone activity over the Tasman Sea, that is, a day is classified as a *Tasman Sea cyclone day* if more than 10% of grid points of cyclone day flag fields within the Tasman Sea (black box in Fig.9; 30°S-45°S, 153°E-170°E) are identified as cyclone-affected (flagged as 1); otherwise, it is classified as a non-cyclone day (flagged as 0). Based on these classified Tasman Sea cyclone and non-cyclone days, a simple rainfall anomaly decomposition scheme is applied. Specifically, for precipitation over any given sample space with n days, the mean precipitation is defined as $P = \frac{1}{n}\sum_{i=1}^{n} p_i$, where p_i denotes the precipitation on the day i. Considering the classification of Tasman Sea cyclone and non-cyclone days, the summation can be separated into two components corresponding to precipitation occurring on cyclone days (p_i^c) and non-cyclone days (p_i^{nc}). If the total number of Tasman Sea cyclone days within this sample space is m, the mean precipitation can be re-written as $P = \frac{1}{n}\left(\sum_{i=1}^{m} p_i^c + \sum_{i=1}^{n-m} p_i^{nc}\right)$, which can be expressed as $P = P^c + P^{nc}$, where $P^c = \frac{1}{n}\sum_{i=1}^{m} p_i^c$ and $P^{nc} = \frac{1}{n}\sum_{i=1}^{n-m} p_i^{nc}$. The two terms represent the contributions of rainfall from Tasman Sea cyclone days and non-cyclone days to the mean rainfall within this sample space, respectively. On this basis, applying this decomposition to all extended SON days during 1979-2022, the climatological mean rainfall can be written as $P_{clim} = P_{clim}^c + P_{clim}^{nc}$, where P_{clim}^c and P_{clim}^{nc} denote the contributions of rainfall from Tasman Sea cyclone and non-cyclone days to the climatological mean rainfall. Similarly, for ENSO-related pattern days, the mean rainfall can be expressed as $P_{ENSOpattern} = P_{ENSOpattern}^c + P_{ENSOpattern}^{nc}$. Therefore, the pattern-day rainfall anomaly (P_{anom}) relative to climatology is given by $P_{anom} = P_{ENSOpattern} - P_{clim}$, which can be decomposed into two components: $P_{anom} = \underbrace{\left(P_{ENSOpattern}^c - P_{clim}^c\right)}_{P_{anom}^c} + \underbrace{\left(P_{ENSOpattern}^{nc} - P_{clim}^{nc}\right)}_{P_{anom}^{nc}}$, with the two bracket terms (denoted by P_{anom}^c and P_{anom}^{nc}) representing the rainfall anomalies associated with changes in Tasman Sea cyclone and non-cyclone days, respectively.

https://doi.org/10.5194/egusphere-2026-3344
Preprint. Discussion started: 14 July 2026

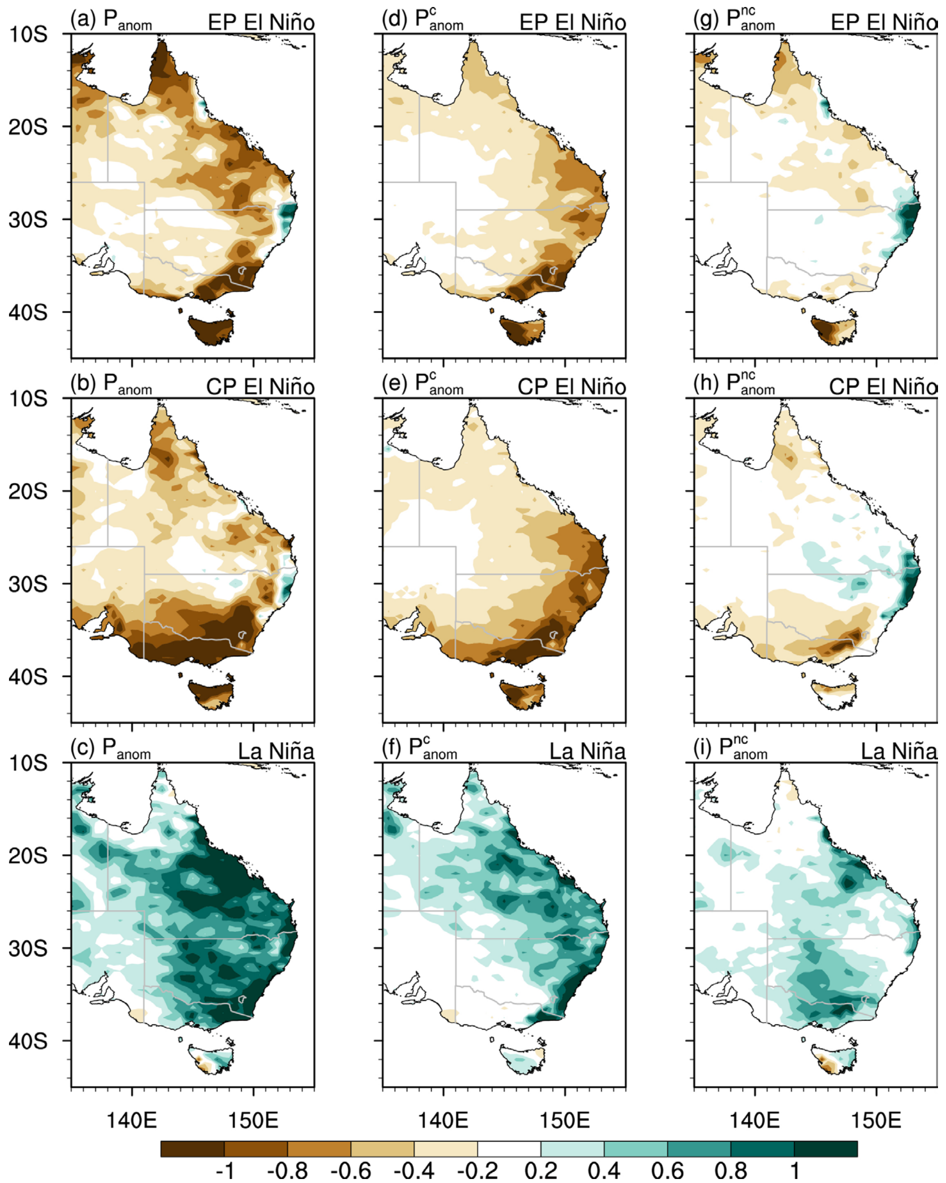

Figure 13. Decomposition of rainfall anomalies (units: mm/day) over eastern Australia during ENSO teleconnection pattern days. Rainfall anomalies of ENSO teleconnection pattern days (P_{anom}; a-c), and the components of rainfall anomalies associated with the changes in Tasman Sea cyclone days (P^{c}_{anom}; d-f) and non-cyclone days (P^{nc}_{anom}; g-i) during EP El Niño (top), CP El Niño (middle), and La Niña (bottom) teleconnection pattern days.

The decomposition described above is applied to the eastern Australian rainfall during EP El Niño-, CP El Niño-, and La Niña-related teleconnection pattern days, and the results are shown in Fig. 13. The pattern-day rainfall anomalies over the eastern Australian region (Fig. 13a-c) are consistent with the composited rainfall anomaly fields shown previously (Fig. 12d-f). Within

https://doi.org/10.5194/egusphere-2026-3344
Preprint. Discussion started: 14 July 2026

these pattern days, the rainfall anomalies associated with the changes in Tasman Sea cyclone days (Fig. 13d-f) exhibit broadly similar spatial structures and comparable magnitudes with the overall pattern-day rainfall anomalies (Fig. 13a-c), especially along the southeastern Australian coast. In contrast, the rainfall anomalies associated with non-cyclone days (Fig. 13g-i) generally exhibit different spatial patterns that do not resemble the overall pattern-day rainfall anomalies, although some localized anomalies are also evident. These results indicate that the rainfall anomalies of ENSO-related pattern days are largely related to changes in cyclone activity, such that enhanced (suppressed) cyclone activity over the Tasman Sea is associated with increased (decreased) eastern Australian rainfall during the established period of La Niña-related (El Niño-related) low-frequency teleconnections. However, it should be noted that, under El Niño conditions, a localized increase in rainfall associated with non-cyclone days appears along the northeastern coast of New South Wales (Fig. 13g, h). This feature is also manifested in the pattern-day results but confined to a relatively small region (Fig. 13a, b), and this is reminiscent of the "Wet East Coast Cluster 3" identified by Hauser et al. (2020), which is argued to be linked to enhanced blocking south of Australia and the occurrence of upper-level cut-off lows affecting the East Coast. In addition, this localized rainfall response is also consistent with previous studies suggesting that ENSO's impacts on the eastern seaboard of Australia can be affected by Indian Ocean-related teleconnections (Pepler et al., 2014a).

Sensitivity tests using alternative grid-points thresholds (e.g., 15% or 20%) for defining Tasman Sea cyclone days yield similar results (Fig. S3), indicating that the findings are robust to the choice of threshold within a reasonable range. Taken together, these results suggest that, within ENSO-related teleconnection pattern periods, eastern Australian rainfall anomalies are closely associated with in Tasman Sea cyclone changes, though non-cyclone variations (e.g., low-frequency circulation anomalies or other synoptic weather systems) also play a role.

https://doi.org/10.5194/egusphere-2026-3344
Preprint. Discussion started: 14 July 2026

4 Summary and discussion

4.1 Summary

In this study, we use a teleconnection pattern-based approach to detect ENSO-related signals in Australian extratropical cyclone activity. By projecting daily low-frequency circulation fields onto composited teleconnection patterns associated with EP El Niño, CP El Niño, and La Niña events, we identify persistent periods during which ENSO-related teleconnection patterns are well established in the Southern Hemisphere extratropics and use these as a refined sample space for calculating cyclone day frequency. Through validating the identified pattern periods from both statistical and dynamical perspectives, together with comparing the results across different sample spaces and examining associated environmental factors, we demonstrate that the emerging signals captured by the pattern-based approach are physically meaningful rather than methodological artifacts. Overall, this approach effectively enhances the signal-to-noise ratio of ENSO-related cyclone variability relative to conventional seasonal-window analyses, revealing significant signals of cyclone activity changes that are episodically modulated by ENSO when the associated low-frequency teleconnection patterns are well established.

The results conditioned on ENSO-related teleconnection pattern days reveal significant cyclone activity anomalies across the Southern Hemisphere extratropics, with the signal emerging over the Tasman Sea, where the changes in cyclone day frequency reach up to about 10% relative to climatology. Specifically, under La Niña pattern days, enhanced cyclone activity over the Tasman Sea is manifested in both increased local cyclogenesis frequency and prolonged cyclone residence time, favoured by anomalous ascent and moisture convergence over the region associated with the La Niña-related large-scale circulation pattern. In contrast, El Niño pattern days exhibit a decrease in cyclone day frequency over the Tasman Sea, particularly for the Central Pacific type, which is consistent with an unfavourable cyclone development environment characterized by anomalous descent and moisture divergence there. Furthermore, a simple decomposition of rainfall anomalies between Tasman Sea cyclone and non-cyclone days highlights the importance of cyclone activity changes in eastern Australian rainfall variability during ENSO-related teleconnection pattern periods. Based on these results, a process-based storyline of ENSO impacts on Australian spring rainfall can be outlined from a combined perspective of weather and climate dynamics: ENSO affects the low-frequency teleconnection patterns, which in turn modulate synoptic cyclone activity over the Tasman Sea, contributing to rainfall anomalies over eastern Australia.

4.2 Discussion

As a key contrast, the absence of regional ENSO-related signal in Australian extratropical cyclones under conventional seasonal analyses can be understood in terms of the intermittent nature of ENSO's extratropical teleconnections on daily timescale. As shown in this study, unsurprisingly, ENSO-related low-frequency circulation patterns are not maintained throughout the whole season but episodically occur with significant regional signatures during specific periods, which is associated with the transience of anomalous tropical convection modulated by ENSO, the time required for Rossby wave

https://doi.org/10.5194/egusphere-2026-3344
Preprint. Discussion started: 14 July 2026

propagation, and the interference of atmospheric internal variability. Importantly, given that the pattern-based results retain the large-scale structure of conventional seasonal anomalies composited by ENSO events, the regional signals (e.g., over the Tasman Sea) that emerge under the pattern-based conditioning should be interpreted as a refinement of the seasonal-based results, rather than a contradiction. This interpretation is supported by previous studies that have documented similar ENSO-related signal. For example, Favre et al. (2012) showed that the frequency of cut-off lows is related to ENSO on interannual timescales, with more systems occurring during La Niña events, particularly at lower latitudes (17.5°S-30°S) in the Australia-South Pacific sector. The increased cyclone frequency over the Tasman Sea during La Niña-related pattern days identified in this study, to some degree, is in agreement with their finding. Therefore, this teleconnection pattern-based approach provides a useful perspective on the weather-climate linkage study which can also be applied to examine the modulation of other large-scale climate modes on extratropical weather systems.

However, unlike conventional seasonal analyses, the present approach does not offer a seasonal estimate of cyclone statistics, since the cyclone day frequency examined here represents a conditional probability restricted to periods when ENSO-related teleconnection patterns are well established in the extratropics. This raises concerns regarding the subseasonal dynamics and predictability of extratropical low-frequency teleconnections under different ENSO backgrounds. In terms of dynamics, as noted in the introduction, low-frequency variability in the extratropical atmosphere is inherently coupled with high-frequency synoptic eddies, forming a two-way interaction. This highlights the need to deepen the understanding of the respective roles of tropical diabatic heating forcing and extratropical transient eddy feedback in the development, maintenance, and decay of ENSO-related low-frequency circulation regimes in the Southern Hemisphere. In terms of predictability, it is necessary to systematically assess the subseasonal predictability and forecast skill of ENSO-related extratropical teleconnections to the Southern Hemisphere in state-of-the-art climate prediction systems (e.g., ACCESS-S2). Overall, improving the representation of ENSO-related extratropical teleconnection patterns in models, together with strengthening the monitoring of tropical convection anomalies, would be beneficial for a better long-range forecast of occurrence probability of high-impact weather events under ENSO conditions.

It is also of value to evaluate ENSO impacts on Southern Hemisphere cyclones using high-resolution model simulations, which is part of our ongoing work. On this basis, it will be particularly interesting to examine how the diverse ENSO teleconnection patterns in the Southern Hemisphere extratropics may change in a warmer climate, and whether their associated modulation on Australian extratropical cyclones could become stronger, to the extent that ENSO-related signals in cyclone activity become more detectable even within seasonal windows.

https://doi.org/10.5194/egusphere-2026-3344
Preprint. Discussion started: 14 July 2026

Code and data availability

The surface cyclone dataset used in this study is attributed to Sprenger et al. (2017) and is available from the authors upon request. AGCD rainfall dataset (Evans et al., 2020) can be obtained from the Australian Bureau of Meteorology (https://www.bom.gov.au/climate/austmaps/about-agcd-maps.shtml). ERA5 reanalysis data (Hersbach et al., 2020) are publicly available from the European Centre for Medium-Range Weather Forecasts (ECMWF) at https://www.ecmwf.int/en/forecasts/dataset/ecmwf-reanalysis-v5. The HadISST dataset (Rayner et al., 2003) is available at https://www.metoffice.gov.uk/hadobs/hadisst/data/download.html. ONI can be accessed at https://www.cpc.ncep.noaa.gov/data/indices/oni.ascii.txt. The interpolated OLR dataset (Liebmann and Smith, 1996) is available at https://psl.noaa.gov/data/gridded/data.olrcdr.interp.html. Data analysis and figure plotting were performed using the NCAR Command Language (NCL) and Python. The associated code scripts are available at https://github.com/Linyuan-Sun/ENSO-AUS-cyclone-WCD-paper.git.

Author contributions

L. S. conceptualized the study, conducted the data analysis and figure plotting, and wrote the original draft. A. S. T., S. M., and L. V. A. supervised the study and contributed to the analysis, validation, and interpretation of the results. C. J. collected and organized the surface cyclone dataset and participated in internal discussions. All authors contributed to the revision of the manuscript.

Competing interests

The contact author has declared that none of the authors has any competing interests.

Acknowledgements

The authors acknowledge support from the Australian Research Council (ARC) Centre of Excellence for the Weather of the 21st Century (CE230100012). A. S. T. and S. M. also acknowledge support from the Australian Government's National Environmental Science Program (NESP). The authors especially thank Michael Sprenger and Heini Wernli for producing the cyclone dataset based on their proposed algorithm and making the data available. L. S. also thanks Mandy Freund, Thomas Spengler, and Ingo Richter for helpful discussions during this study. This work used resources and services from the Australian National Computational Infrastructure (NCI).

https://doi.org/10.5194/egusphere-2026-3344
Preprint. Discussion started: 14 July 2026

Financial support

This research has been supported by the ARC Centre of Excellence for 21st Century Weather (CE230100012).

https://doi.org/10.5194/egusphere-2026-3344
Preprint. Discussion started: 14 July 2026

References

Benedict, J. J., Lee, S., and Feldstein, S. B.: Synoptic view of the North Atlantic Oscillation, J. Atmos. Sci., 61, 121–144, https://doi.org/10.1175/1520-0469(2004)061<0121:SVOTNA>2.0.CO;2, 2004.

Bjerknes, J.: Atmospheric Teleconnections From the Equatorial Pacific, Mon. Weather Rev., 97, 163–172, 1969.

Branstator, G.: Long-lived response of the midlatitude circulation and storm tracks to pulses of tropical heating, J. Clim., 27, 8809–8826, https://doi.org/10.1175/JCLI-D-14-00312.1, 2014.

Bretherton, C. S., Widmann, M., Dymnikov, V. P., Wallace, J. M., and Bladé, I.: The Effective Number of Spatial Degrees of Freedom of a Time-Varying Field, J. Clim., 12, 1990–2009, https://doi.org/10.1175/1520-0442(1999)012<1990:TENOSD>2.0.CO;2, 1999.

Cai, W., van Rensch, P., Cowan, T., and Hendon, H. H.: Teleconnection pathways of ENSO and the IOD and the mechanisms for impacts on Australian rainfall, J. Clim., 24, 3910–3923, https://doi.org/10.1175/2011JCLI4129.1, 2011.

Chand, S. S., Dowdy, A. J., Ramsay, H. A., Walsh, K. J. E., Tory, K. J., Power, S. B., Bell, S. S., Lavender, S. L., Ye, H., and Kuleshov, Y.: Review of tropical cyclones in the Australian region: Climatology, variability, predictability, and trends, Wiley Interdiscip. Rev. Clim. Chang., 10, 1–17, https://doi.org/10.1002/wcc.602, 2019.

Cowan, T., Van Rensch, P., Purich, A., and Cai, W.: The association of tropical and extratropical climate modes to atmospheric blocking across southeastern Australia, J. Clim., 26, 7555–7569, https://doi.org/10.1175/JCLI-D-12-00781.1, 2013.

Cowan, T., Wheeler, M. C., and Marshall, A. G.: The Combined Influence of the Madden-Julian Oscillation and El Niño-Southern Oscillation on Australian Rainfall, J. Clim., 36, 313–334, https://doi.org/10.1175/JCLI-D-22-0357.1, 2023.

Deser, C., Simpson, I. R., McKinnon, K. A., and Phillips, A. S.: The Northern Hemisphere Extratropical Atmospheric Circulation Response to ENSO: How Well Do We Know It and How Do We Evaluate Models Accordingly?, J. Clim., 30, 5059–5082, https://doi.org/10.1175/JCLI-D-16-0844.1, 2017.

Dole, R. M.: Linking Weather and Climate, Meteorol. Monogr., 55, 297–348, https://doi.org/10.1175/0065-9401-33.55.297, 2008.

Dole, R. M. and Gordon, N. D.: Persistent Anomalies of the Extratropical Northern Hemisphere Wintertime Circulation: Geographical Distribution and Regional Persistence Characteristics, Mon. Weather Rev., 111, 1567–1586, https://doi.org/10.1175/1520-0493(1983)111<1567:PAOTEN>2.0.CO;2, 1983.

Dowdy, A. J., Mills, G. A., Timbal, B., and Wang, Y.: Changes in the risk of extratropical cyclones in eastern Australia, J.

https://doi.org/10.5194/egusphere-2026-3344
Preprint. Discussion started: 14 July 2026

Clim., 26, 1403–1417, https://doi.org/10.1175/JCLI-D-12-00192.1, 2013.

Duchon, C. E.: Lanczos Filtering in One and Two Dimensions, J. Appl. Meteorol., 18, 1016–1022, https://doi.org/10.1175/1520-0450(1979)018<1016:LFIOAT>2.0.CO;2, 1979.

Evans, A., Jones, D., Smalley, R., and Lellyett, S.: An enhanced gridded rainfall dataset scheme for Australia, 41 pages pp., 2020.

Favre, A., Hewitson, B., Tadross, M., Lennard, C., and Cerezo-Mota, R.: Relationships between cut-off lows and the semiannual and southern oscillations, Clim. Dyn., 38, 1473–1487, https://doi.org/10.1007/s00382-011-1030-4, 2012.

Feldstein, S. B.: The timescale, power spectra, and climate noise properties of teleconnection patterns, J. Clim., 13, 4430–4440, https://doi.org/10.1175/1520-0442(2000)013<4430:TTPSAC>2.0.CO;2, 2000.

Franzke, C., Feldstein, S. B., and Lee, S.: Synoptic analysis of the Pacific-North American teleconnection pattern, Q. J. R. Meteorol. Soc., 137, 329–346, https://doi.org/10.1002/qj.768, 2011.

Gillett, Z. E., Taschetto, A. S., Holgate, C. M., and Santoso, A.: Linking ENSO to Synoptic Weather Systems in Eastern Australia, Geophys. Res. Lett., 50, 1–9, https://doi.org/10.1029/2023GL104814, 2023.

Grant, M. O., Ukkola, A. M., Vogel, E., Hobeichi, S., Pitman, A. J., Borowiak, A. R., and Fowler, K.: Historical trends of seasonal droughts in Australia, Hydrol. Earth Syst. Sci., 29, 5555–5573, https://doi.org/10.5194/hess-29-5555-2025, 2025.

Grosfeld, N. H., McGregor, S., and Taschetto, A. S.: An Automated Climatology of Cool-Season Cutoff Lows over Southeastern Australia and Relationships with the Remote Climate Drivers, Mon. Weather Rev., 149, 4167–4181, https://doi.org/10.1175/MWR-D-21-0142.1, 2021.

Hannachi, A., Straus, D. M., Franzke, C. L. E., Corti, S., and Woollings, T.: Low-frequency nonlinearity and regime behavior in the Northern Hemisphere extratropical atmosphere, Rev. Geophys., 55, 199–234, https://doi.org/10.1002/2015RG000509, 2017.

Hauser, S., Grams, C. M., Reeder, M. J., McGregor, S., Fink, A. H., and Quinting, J. F.: A weather system perspective on winter–spring rainfall variability in southeastern Australia during El Niño, Q. J. R. Meteorol. Soc., 146, 2614–2633, https://doi.org/10.1002/qj.3808, 2020.

Held, I. M., Ting, M., and Wang, H.: Northern winter stationary waves: Theory and modeling, J. Clim., 15, 2125–2144, https://doi.org/10.1175/1520-0442(2002)015<2125:NWSWTA>2.0.CO;2, 2002.

Hersbach, H., Bell, B., Berrisford, P., Hirahara, S., Horányi, A., Muñoz-Sabater, J., Nicolas, J., Peubey, C., Radu, R., Schepers, D., Simmons, A., Soci, C., Abdalla, S., Abellan, X., Balsamo, G., Bechtold, P., Biavati, G., Bidlot, J.,

https://doi.org/10.5194/egusphere-2026-3344
Preprint. Discussion started: 14 July 2026

Bonavita, M., De Chiara, G., Dahlgren, P., Dee, D., Diamantakis, M., Dragani, R., Flemming, J., Forbes, R., Fuentes, M., Geer, A., Haimberger, L., Healy, S., Hogan, R. J., Hólm, E., Janisková, M., Keeley, S., Laloyaux, P., Lopez, P., Lupu, C., Radnoti, G., de Rosnay, P., Rozum, I., Vamborg, F., Villaume, S., and Thépaut, J. N.: The ERA5 global reanalysis, Q. J. R. Meteorol. Soc., 146, 1999–2049, https://doi.org/10.1002/qj.3803, 2020.

Hoerling, M. P. and Kumar, A.: Atmospheric response patterns associated with tropical forcing, J. Clim., 15, 2184–2203, https://doi.org/10.1175/1520-0442(2002)015<2184:ARPAWT>2.0.CO;2, 2002.

Holgate, C., Evans, J. P., Taschetto, A. S., Gupta, A. Sen, and Santoso, A.: The Impact of Interacting Climate Modes on East Australian Precipitation Moisture Sources, J. Clim., 35, 3147–3159, https://doi.org/10.1175/JCLI-D-21-0750.1, 2022.

Holgate, C. M., Falster, G. M., Gillett, Z. E., Goswami, P., Grant, M. O., Hobeichi, S., Hoffmann, D., Jiang, X., Jin, C., Lu, X., Mu, M., Page, J. C., Parker, T. J., Vogel, E., Abram, N. J., Evans, J. P., Gallant, A. J. E., Henley, B. J., Kala, J., King, A. D., Maher, N., Nguyen, H., Pitman, A. J., Power, S. B., Rauniyar, S. P., Taschetto, A. S., and Ukkola, A. M.: Physical mechanisms of meteorological drought development, intensification and termination: an Australian review, Commun. Earth Environ., 6, 220, https://doi.org/10.1038/s43247-025-02179-3, 2025.

Hoskins, B. J. and Karoly, D. J.: The Steady Linear Response of a Spherical Atmosphere to Thermal and Orographic Forcing, J. Atmos. Sci., 38, 1179–1196, https://doi.org/10.1175/1520-0469(1981)038<1179:TSLROA>2.0.CO;2, 1981.

Jaffe, S. C., Martin, J. E., Vimont, D. J., and Lorenz, D. J.: A synoptic climatology of episodic, subseasonal retractions of the Pacific jet, J. Clim., 24, 2846–2860, https://doi.org/10.1175/2010JCLI3995.1, 2011.

Jin, C., Reeder, M. J., Gallant, A. J. E., Parker, T., and Sprenger, M.: Changes in Weather Systems during Anomalously Wet and Dry Years in Southeastern Australia, J. Clim., 37, 1131–1153, https://doi.org/10.1175/JCLI-D-23-0305.1, 2024.

Jin, C., Gallant, A. J. E., Parker, T., and Reeder, M. J.: Weather systems and their contribution to seasonal rainfall in Australia, Q. J. R. Meteorol. Soc., 151, 1–22, https://doi.org/10.1002/qj.5013, 2025.

Jin, F. F., Pan, L. L., and Watanabe, M.: Dynamics of synoptic eddy and low-frequency flow interaction. Part I: A linear closure, J. Atmos. Sci., 63, 1677–1694, https://doi.org/10.1175/JAS3715.1, 2006.

Karoly, D. J.: Southern Hemisphere Circulation Features Associated with El Niño-Southern Oscillation Events, J. Clim., 2, 1239–1252, https://doi.org/10.1175/1520-0442(1989)002<1239:SHCFAW>2.0.CO;2, 1989.

Karoly, D. J.: The role of transient eddies in low-frequency zonal variations of the Southern Hemisphere circulation, Tellus, Ser. A, 42 A, 41–50, https://doi.org/10.3402/tellusa.v42i1.11858, 1990.

Kug, J. S., Jin, F. F., and An, S. Il: Two types of El Niño events: Cold tongue El Niño and warm pool El Niño, J. Clim., 22, 1499–1515, https://doi.org/10.1175/2008JCLI2624.1, 2009.

L'Heureux, M. L., Tippett, M. K., Wheeler, M. C., Nguyen, H., Narsey, S., Johnson, N., Hu, Z. Z., Watkins, A. B., Lucas, C., Ganter, C., Becker, E., Wang, W., and Di Liberto, T.: A Relative Sea Surface Temperature Index for Classifying ENSO Events in a Changing Climate, J. Clim., 37, 1197–1211, https://doi.org/10.1175/JCLI-D-23-0406.1, 2024.

Lau, N.-C. and Holopainen, E. O.: Transient Eddy Forcing of the Time-Mean Flow as Identified by Geopotential Tendencies, J. Atmos. Sci., 41, 313–328, https://doi.org/10.1175/1520-0469(1984)041<0313:TEFOTT>2.0.CO;2, 1984.

Li, Y. and Lau, N. C.: Contributions of downstream eddy development to the teleconnection between ENSO and the atmospheric circulation over the North Atlantic, J. Clim., 25, 4993–5010, https://doi.org/10.1175/JCLI-D-11-00377.1, 2012.

Liebmann, B. and Smith, C. A.: Description of a Complete (Interpolated) Outgoing Longwave Radiation Dataset, Bull. Am. Meteorol. Soc., 77, 1275–1277, 1996.

Lindzen, R. S. and Farrell, B.: A simple approximate result for the maximum growth rate of baroclinic instabilities., J. Atmos. Sci., 37, 1648–1654, https://doi.org/10.1175/1520-0469(1980)037<1648:ASARFT>2.0.CO;2, 1980.

Liu, Z. and Wang, L.: Enhanced Occurrence of Atmospheric Blocking in the Southern Hemisphere by Baroclinic Annular Mode, Geophys. Res. Lett., 51, https://doi.org/10.1029/2023GL107343, 2024.

Lorenz, E. N.: Deterministic Nonperiodic Flow, J. Atmos. Sci., 20, 130–141, https://doi.org/10.1175/1520-0469(1963)020<0130:DNF>2.0.CO;2, 1963.

Ma, Y., Sun, J., Dong, T., Yu, W., and Dong, W.: More profound impact of CP ENSO on Australian spring rainfall in recent decades, Clim. Dyn., 60, 3065–3079, https://doi.org/10.1007/s00382-022-06485-w, 2023.

Mariani, M., Fletcher, M. S., Holz, A., and Nyman, P.: ENSO controls interannual fire activity in southeast Australia, Geophys. Res. Lett., 43, 10,891-10,900, https://doi.org/10.1002/2016GL070572, 2016.

Matthews, A. J. and Kiladis, G. N.: Interactions between ENSO, transient circulation, and tropical convection over the Pacific, J. Clim., 12, 3062–3086, https://doi.org/10.1175/1520-0442(1999)012<3062:IBETCA>2.0.CO;2, 1999.

McBride, J. L. and Nicholls, N.: Seasonal Relationships between Australian Rainfall and the Southern Oscillation, Mon. Weather Rev., 111, 1998–2004, https://doi.org/10.1175/1520-0493(1983)111<1998:SRBARA>2.0.CO;2, 1983.

McGregor, S., Gallant, A., and van Rensch, P.: Quantifying ENSOs Impact on Australia's Regional Monthly Rainfall Risk, Geophys. Res. Lett., 51, https://doi.org/10.1029/2023GL106298, 2024.

Mo, K. C.: Relationships between low-frequency variability in the Southern Hemisphere and sea surface temperature

https://doi.org/10.5194/egusphere-2026-3344
Preprint. Discussion started: 14 July 2026

anomalies, J. Clim., 13, 3599–3610, https://doi.org/10.1175/1520-0442(2000)013<3599:RBLFVI>2.0.CO;2, 2000.

Mo, K. C. and Higgins, R. W.: The Pacific-South American modes and tropical convection during the Southern Hemisphere winter, Mon. Weather Rev., 126, 1581–1596, https://doi.org/10.1175/1520-0493(1998)126<1581:TPSAMA>2.0.CO;2, 1998.

Murphy, B. F. and Timbal, B.: A review of recent climate variability and climate change in Southeastern Australia, Int. J. Climatol., 28, 859–879, https://doi.org/10.1002/joc.1627, 2008.

Neu, U., Akperov, M. G., Bellenbaum, N., Benestad, R., Blender, R., Caballero, R., Cocozza, A., Dacre, H. F., Feng, Y., Fraedrich, K., Grieger, J., Gulev, S., Hanley, J., Hewson, T., Inatsu, M., Keay, K., Kew, S. F., Kindem, I., Leckebusch, G. C., Liberato, M. L. R., Lionello, P., Mokhov, I. I., Pinto, J. G., Raible, C. C., Reale, M., Rudeva, I., Schuster, M., Simmonds, I., Sinclair, M., Sprenger, M., Tilinina, N. D., Trigo, I. F., Ulbrich, S., Ulbrich, U., Wang, X. L., and Wernli, H.: Imilast: A community effort to intercompare extratropical cyclone detection and tracking algorithms, Bull. Am. Meteorol. Soc., 94, 529–547, https://doi.org/10.1175/BAMS-D-11-00154.1, 2013.

Nicholls, N.: A Possible Method for Predicting Seasonal Tropical Cyclone Activity in the Australian Region, Mon. Weather Rev., 107, 1221–1224, https://doi.org/10.1175/1520-0493(1979)107<1221:APMFPS>2.0.CO;2, 1979.

Pepler, A. and Dowdy, A.: Intense east coast lows and associated rainfall in eastern Australia, J. South. Hemisph. Earth Syst. Sci., 71, 110–122, https://doi.org/10.1071/ES20013, 2021.

Pepler, A., Timbal, B., Rakich, C., and Coutts-Smith, A.: Indian ocean dipole overrides ENSO's influence on cool season rainfall across the Eastern seaboard of Australia, J. Clim., 27, 3816–3826, https://doi.org/10.1175/JCLI-D-13-00554.1, 2014a.

Pepler, A., Coutts-Smith, A., and Timbal, B.: The role of East Coast Lows on rainfall patterns and inter-annual variability across the East Coast of Australia, Int. J. Climatol., 34, 1011–1021, https://doi.org/10.1002/joc.3741, 2014b.

Pepler, A. S., Alexander, L. V., Evans, J. P., and Sherwood, S. C.: The influence of local sea surface temperatures on Australian east coast cyclones, J. Geophys. Res., 121, 13,352-13,363, https://doi.org/10.1002/2016JD025495, 2016.

Pook, M. J., McIntosh, P. C., and Meyers, G. A.: The synoptic decomposition of cool-season rainfall in the southeastern Australian cropping region, J. Appl. Meteorol. Climatol., 45, 1156–1170, https://doi.org/10.1175/JAM2394.1, 2006.

Power, S., Casey, T., Folland, C., Colman, A., and Mehta, V.: Inter-decadal modulation of the impact of ENSO on Australia, Clim. Dyn., 15, 319–324, https://doi.org/10.1007/s003820050284, 1999.

Ramsay, H. A., Richman, M. B., and Leslie, L. M.: Seasonal tropical cyclone predictions using optimized combinations of ENSO regions: Application to the coral sea basin, J. Clim., 27, 8527–8542, https://doi.org/10.1175/JCLI-D-14-00017.1, 2014.

https://doi.org/10.5194/egusphere-2026-3344
Preprint. Discussion started: 14 July 2026

Randall, D. A. and Emanuel, K.: The Weather–Climate Schism, Bull. Am. Meteorol. Soc., 105, E300–E305, https://doi.org/10.1175/BAMS-D-23-0124.1, 2024.

Rayner, N. A., Parker, D. E., Horton, E. B., Folland, C. K., Alexander, L. V., Rowell, D. P., Kent, E. C., and Kaplan, A.: Global analyses of sea surface temperature, sea ice, and night marine air temperature since the late nineteenth century, J. Geophys. Res. Atmos., 108, 4407, https://doi.org/10.1029/2002JD002670, 2003.

van Rensch, P., McGregor, S., and Gallant, A.: The Extent of El Niño and La Niña Influence on Australian Rainfall, Geophys. Res. Lett., 53, 1–10, https://doi.org/10.1029/2025GL118454, 2026.

Risbey, J. S., Pook, M. J., McIntosh, P. C., Wheeler, M. C., and Hendon, H. H.: On the remote drivers of rainfall variability in Australia, Mon. Weather Rev., 137, 3233–3253, https://doi.org/10.1175/2009MWR2861.1, 2009.

Santoso, A., Hendon, H., Watkins, A., Power, S., Dommenget, D., England, M. H., Frankcombe, L., Holbrook, N. J., Holmes, R., Hope, P., Lim, E. P., Luo, J. J., McGregor, S., Neske, S., Nguyen, H., Pepler, A., Rashid, H., Gupta, A. Sen, Taschetto, A. S., Wang, G., Abellán, E., Sullivan, A., Huguenin, M. F., Gamble, F., and Delage, F.: Dynamics and predictability of El Niño-Southern oscillation: An Australian perspective on progress and challenges, Bull. Am. Meteorol. Soc., 100, 403–420, https://doi.org/10.1175/BAMS-D-18-0057.1, 2019.

Sardeshmukh, P. D. and Hoskins, B. J.: The Generation of Global Rotational Flow by Steady Idealized Tropical Divergence, J. Atmos. Sci., 45, 1228–1251, https://doi.org/10.1175/1520-0469(1988)045<1228:TGOGRF>2.0.CO;2, 1988.

Simmons, A. J. and Hoskins, B. J.: The Downstream and Upstream Development of Unstable Baroclinic Waves, J. Atmos. Sci., 36, 1239–1254, https://doi.org/10.1175/1520-0469(1979)036<1239:TDAUDO>2.0.CO;2, 1979.

Song, J.: Understanding anomalous synoptic eddy vorticity forcing in Pacific-North American teleconnection pattern events, J. Atmos. Sci., 75, 4287–4312, https://doi.org/10.1175/JAS-D-18-0071.1, 2018.

Sprenger, M., Fragkoulidis, G., Binder, H., Croci-Maspoli, M., Graf, P., Grams, C. M., Knippertz, P., Madonna, E., Schemm, S., Škerlak, B., and Wernli, H.: Global climatologies of Eulerian and Lagrangian flow features based on ERA-Interim, Bull. Am. Meteorol. Soc., 98, 1739–1748, https://doi.org/10.1175/BAMS-D-15-00299.1, 2017.

Stan, C., Straus, D. M., Frederiksen, J. S., Lin, H., Maloney, E. D., and Schumacher, C.: Review of Tropical-Extratropical Teleconnections on Intraseasonal Time Scales, Rev. Geophys., 55, 902–937, https://doi.org/10.1002/2016RG000538, 2017.

Sun, L., S. Taschetto, A., McGregor, S., and Alexander, L. V: Diverse Impacts of Eastern Pacific and Central Pacific ENSO on Australian Spring Rainfall and Associated Southern Hemisphere Large-scale Circulation, J. Clim., 1–46, https://doi.org/10.1175/JCLI-D-25-0606.1, 2026.

Tamarin-Brodsky, T., Harnik, N., and Falkena, S. K. J.: On Storm Tracks, Weather Regimes, and a Wave Breaking Recipe,

https://doi.org/10.5194/egusphere-2026-3344
Preprint. Discussion started: 14 July 2026

AGU Adv., 7, https://doi.org/10.1029/2025AV002049, 2026.

Taschetto, A. S., Ummenhofer, C. C., Stuecker, M. F., Dommenget, D., Ashok, K., Rodrigues, R. R., and Yeh, S.: ENSO Atmospheric Teleconnections, in: El Niño Southern Oscillation in a Changing Climate, 309–335, 2020.

Taschetto, A. S., McGregor, S., Dommenget, D., Gillett, Z. E., Nicholls, N., Sharmila, S., van Rensch, P., Verdon-Kidd, D., Boschat, G., Chung, C., Lieber, R., Abram, N., Allan, R., Allen, K., Ashcroft, L., Brown, J. R., Cai, W., Chand, S., Cowan, T., Dao, T. L., de Burgh-Day, C., Freund, M. B., Gallant, A., Gergis, J., Holbrook, N. J., Heidemann, H., Holgate, C., Hope, P., King, A., Lim, E.-P., McBride, J. L., McKay, R. C., Nguyen, H., Pepler, A., Perkins-Kirkpatrick, S., Power, S., Risbey, J. S., Santoso, A., Ummenhofer, C. C., Wang, G., and Zhang, X.: Climate impacts of the El Niño–Southern Oscillation on Australia, Nat. Rev. Earth Environ., https://doi.org/10.1038/s43017-025-00747-x, 2025.

Thorncroft, C. D., Hoskins, B. J., and McIntyre, M. E.: Two paradigms of baroclinic-wave life-cycle behaviour, Q. J. R. Meteorol. Soc., 119, 17–55, https://doi.org/10.1002/qj.49711950903, 1993.

Trascasa-Castro, P., Maycock, A. C., Ruprich-Robert, Y., Turco, M., and Staten, P. W.: Atlantic Multidecadal Variability modulates the climate impacts of El Niño–Southern Oscillation in Australia, Environ. Res. Lett., 18, 084029, https://doi.org/10.1088/1748-9326/ace920, 2023.

Trenberth, K. E., Branstator, G. W., Karoly, D., Kumar, A., Lau, N. C., and Ropelewski, C.: Progress during TOGA in understanding and modeling global teleconnections associated with tropical sea surface temperatures, J. Geophys. Res. Ocean., 103, 14291–14324, https://doi.org/10.1029/97jc01444, 1998.

Ummenhofer, C. C., Gupta, A. Sen, Briggs, P. R., England, M. H., McIntosh, P. C., Meyers, G. A., Pook, M. J., Raupach, M. R., and Risbey, J. S.: Indian and Pacific Ocean influences on southeast Australian drought and soil moisture, J. Clim., 24, 1313–1336, https://doi.org/10.1175/2010JCLI3475.1, 2011.

Verdon, D. C., Wyatt, A. M., Kiem, A. S., and Franks, S. W.: Multidecadal variability of rainfall and streamflow: Eastern Australia, Water Resour. Res., 40, 1–8, https://doi.org/10.1029/2004WR003234, 2004.

Walker, G.: CORRELATION IN SEASONAL VARIATIONS OF WEATHER—A FURTHER STUDY OF WORLD WEATHER 1, Mon. Weather Rev., 53, 252–254, https://doi.org/10.1175/1520-0493(1925)53<252:CISVOW>2.0.CO;2, 1925.

Wang, Y., Huang, G., Hu, K., Tao, W., Li, X., Gong, H., Gu, L., and Zhang, W.: Asymmetric Impacts of El Niño and La Niña on the Pacific–South America Teleconnection Pattern, J. Clim., 35, 1825–1838, https://doi.org/10.1175/JCLI-D-21-0285.1, 2022.

Wernli, H. and Schwierz, C.: Surface cyclones in the ERA-40 dataset (1958-2001). Part I: Novel identification method and

https://doi.org/10.5194/egusphere-2026-3344
Preprint. Discussion started: 14 July 2026

global climatology, J. Atmos. Sci., 63, 2486–2507, https://doi.org/10.1175/JAS3766.1, 2006.

Wilks, D. S.: Statistical Methods in the Atmospheric Sciences, Elsevier, 676 pp., https://doi.org/10.1016/C2017-0-03921-6, 2011.

Williams, A. A. J. and Karoly, D. J.: Extreme fire weather in Australia and the impact of the El Niño-Southern Oscillation, Aust. Meteorol. Mag., 48, 15–22, https://doi.org/10.1071/ES99002, 1999.

Wu, W. and Leonard, M.: Impact of ENSO on dependence between extreme rainfall and storm surge, Environ. Res. Lett., 14, https://doi.org/10.1088/1748-9326/ab59c2, 2019.